eDNAPlus: A unifying modelling framework for DNA-based biodiversity monitoring

Alex Diana[1], Eleni Matechou[1], Jim Griffin[2], Douglas W. Yu[3,4], Mingjie Luo[5], Marie Tosa[5], Alex Bush[6], Richard Griffiths[7]

[1] School of Mathematics, Statistics and Actuarial Science, University of Kent, UK,

[2] Department of Statistical Science, University College London, UK,

[3] School of Biological Sciences, University of East Anglia, UK,

[4] Center for Excellence in Animal Evolution and Genetics &
State Key Laboratory of Genetic Resources and Evolution &
Yunnan Key Laboratory of Biodiversity and Ecological Security of Gaoligong Mountain &
Kunming Institute of Zoology, Chinese Academy of Sciences, Kunming, China,

[5] Kunming College of Life Sciences, University of Chinese Academy of Sciences, China,

[6] Department of Fisheries, Wildlife, & Conservation Sciences, Oregon State University, Oregon USA,

[7] Lancaster Environment Centre, University of Lancaster, UK,

[8] Durrell Institute of Conservation and Ecology, University of Kent, UK

Abstract

DNA-based biodiversity surveys, which involve collecting physical samples from survey sites and assaying them in the laboratory to detect species via their diagnostic DNA sequences, are increasingly being adopted for biodiversity monitoring and decision-making. The most commonly employed method, metabarcoding, combines PCR with high-throughput DNA sequencing to amplify and read 'DNA barcode' sequences, generating count data indicating the number of times each DNA barcode was read. However, DNA-based data are noisy and error-prone, with several sources of variation, and cannot alone estimate the species-specific amount of DNA present at a surveyed site (*DNA biomass*). In this paper, we present a unifying modelling framework for DNA-based survey data that allows estimation of *changes in DNA biomass within species, across sites* and their links to environmental covariates, whilst for the first time simultaneously accounting for key sources of variation, error and noise in the data-generating process, and for between-species and between-sites correlation. Bayesian inference is performed using MCMC with Laplace approximations. We describe a re-parameterisation scheme for crossed-effects models designed to improve mixing, and an adaptive approach for updating latent variables, which reduces computation time. Theoretical and simulation results are used to guide study design, including the level of replication at different survey stages and the use of quality control methods. Finally, we demonstrate our new framework on a dataset of Malaise-trap samples, quantifying the effects of elevation and distance-to-road on each species, and produce maps identifying areas of high biodiversity and species DNA biomass.

Keywords: crossed-effects model, environmental DNA, joint species distribution modelling, observation error, occupancy modelling

1 Introduction

Ecology is undergoing a technology revolution that is making it possible to rapidly generate species inventories via automated and high-throughput DNA sequencers and via electronic sensors, such as drones, satellites, camera traps, and acoustic recorders. These techniques can, if coupled with appropriate algorithms and databases, simultaneously identify large numbers of target species, including those that are cryptic, difficult-to-access, tiny, and low-abundance (Bush et al., 2017; Besson et al., 2022; Piper et al., 2019; Ley, 2022). So far, the most efficient method for generating species-resolution inventories is DNA-based surveys, which rely on reading DNA barcodes: short, standardized sections of the genome that can be compared to a reference library to enable taxonomic identifications without the need to examine organism morphologies (Ratnasingham and Hebert, 2007).

DNA barcoding refers to the identification of single species (Hebert et al., 2003), and DNA *meta*barcoding refers to the detection of large numbers of species from environmental DNA (eDNA), which is the collective name for DNA isolated from environmental samples (Taberlet et al., 2018). These environmental samples include water (Thomsen and Willerslev, 2015), soil (Frøslev et al., 2019), air (Clare et al., 2022), and bulk tissue (i.e. mass-trapped organisms) (Ji et al., 2013). For instance, Thomsen and Sigsgaard (2019) demonstrated that traces of eDNA on flower petals could be analysed to describe the diversity of arthropods that visit wildflowers, including pollinators, parasitoids, predators, and herbivores. Ji et al. (2022) used the trace amounts of residual vertebrate blood left in 30,468 blood-sucking leeches to map vertebrate wildlife across a 677 km^2 nature reserve in China. Finally, Abrego et al. (2021) sequenced 542 mixed-species, bulk-tissue samples of arctic arthropods captured over 14 years and showed that species richness in the study site had declined by 50% during a time period in which local mean temperature had increased by 2C.

The potential of DNA-based surveys for monitoring and managing biodiversity comes with a number of statistical challenges. Firstly, species-specific absolute abundances can-

not be estimated using DNA data alone. Secondly, DNA-based surveys yield data that are overdispersed (including zero-inflation) relative to a Poisson distribution due to several types of error and noise (see Section 1.1), some of which are species-specific. The framework presented in this paper addresses these challenges by developing a novel model and corresponding efficient inferential tools. Using our framework, we model *within-species change in DNA biomass across sites* (described in Section 1.1), which under certain conditions can be considered as a proxy for change in abundance, hence addressing the first challenge. To address the second challenge, we propose a hierarchical crossed-effects model that expresses key sources of variation, error and noise in the data collection and analysis pipeline, whilst accounting for correlation across species and across sites, and for covariate effects on DNA biomass. We also model frequently employed controls at the PCR stage and evaluate their effect on inference.

1.1 DNA-based surveys and associated challenges

Each individual of a species sheds tissue and waste products, and thus its DNA, into the environment. We will refer to this as *DNA biomass*. As we explain in Section 2, the estimates of species DNA biomass obtained from DNA-based surveys alone are only meaningful in comparison between sites, and for that reason, in this paper we focus on modelling *changes in DNA biomass within species, across sites*, referred to as changes in DNA biomass throughout. We achieve this by assuming that the processes are standardised across sites, samples, and PCR replicates and that any differences in the efficiencies of the processes are explained by covariates that can be included in the model. We highlight that, theoretically, the overall amount of DNA biomass for each species is proportional to the species' abundance at that site, but the rate at which each species sheds DNA into the environment is unknown and not estimable using eDNA data alone. Additionally, the relationship between DNA biomass and abundance can vary between species and sites due to environmental conditions, such as DNA degradation rates, and we return to this point in Section 6. Under the assumption that this relationship does not vary with sites then we

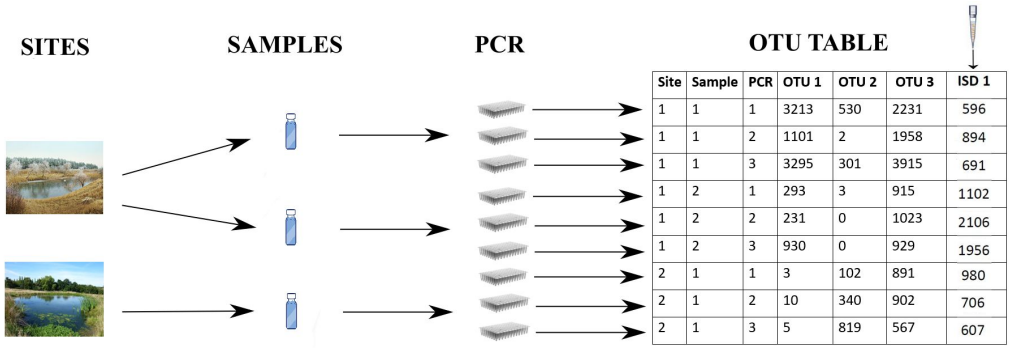

Site	Sample	PCR	OTU 1	OTU 2	OTU 3	ISD 1
1	1	1	3213	530	2231	596
1	1	2	1101	2	1958	894
1	1	3	3295	301	3915	691
1	2	1	293	3	915	1102
1	2	2	231	0	1023	2106
1	2	3	930	0	929	1956
2	1	1	3	102	891	980
2	1	2	10	340	902	706
2	1	3	5	819	567	607

Figure 1: Representation of the DNA biomass collection stage (Stage 1, Sites to Samples) and the DNA biomass analysis stage (Stage 2, Samples to PCR to OTU table). Each of the selected sites to be surveyed hosts a community of species, and hence a certain amount of DNA biomass for each species. One or more physical samples are collected from each surveyed site, and a 'spike-in' or 'internal standard' ISD, can be added to each sample (last column). Each sample is PCR'd one or more times and then sequenced. This process gives rise to the OTU table.

can interpret changes in species DNA biomass as corresponding changes in abundance.

DNA-based surveys comprise two stages (Figure 1): the sample collection stage (Stage 1), taking place in the field, and the sample analysis stage (Stage 2), taking place in the lab.

In Stage 1, physical samples are collected from each surveyed site. However, the amount of DNA biomass of each species collected in each sample is the result of a noisy and error-prone process (see Table 1). Specifically, the sampling method inevitably favours some species over others, and as a result, DNA biomass collection rates, conditional on the available DNA biomasses, are species-specific (*Stage 1 species effect*). The amount of DNA biomass collected for each species also varies between samples collected at the same site (*Stage 1 noise*). Finally, there are non-negligible probabilities that (a) no DNA biomass is collected for a species even if there was DNA biomass of that species at the site (false negative error) and (b) the DNA biomass in the sample is not the result of species presence, but instead reflects contamination or deposition from elsewhere (false positive error) (Stage 1 false negative and false positive errors are jointly referred to as *Stage 1 error*).

In Stage 2, the physical samples are assayed in the lab. The most frequently used method for reading DNA barcodes from eDNA samples is 'amplicon sequencing' (see Lindahl et al.,

2013, for an excellent review). In short, from each sample, all DNA is extracted and purified. After extraction, a small aliquot of DNA from each sample is subjected to Polymerase Chain Reaction (PCR), which selectively amplifies (makes many copies of) just the DNA-barcode sequences. It is common practice in Stage 2 for a sample to be PCR-assayed multiple times, known as technical replicates to distinguish them from sample replicates in Stage 1. The PCR outputs ('amplicons') from all the samples and their technical replicates are pooled and read on a high-throughput DNA sequencer. This procedure ultimately leads to a list of many millions of individual DNA sequences (known as reads), which are processed in a bioinformatic pipeline that removes low-quality reads, groups the remainder into clusters of similar reads that are species hypotheses known as OTUs (Operational Taxonomic Units), and apportions each OTU's reads back to its original samples and PCRs. The resulting *OTU table* dataset indicates the number of reads for each OTU in each PCR in each sample in each site (Figure 1), with columns representing the species and rows representing the PCR runs. For simplicity, we hereafter use the terms OTUs and species interchangeably.

A real-world complication in DNA-based laboratory pipelines is that samples are typically 'normalised' one or more times. For instance, after the samples are enzymatically digested to break down cells and release their DNA into their 'lysis-buffer' solutions, each sample constitutes a larger volume of liquid than can be used for DNA extraction. The samples are thus normalised by taking a fixed volume from each sample for processing. Another normalisation step happens after PCR, because different PCR replicates can generate different amounts of product. In this case, the PCR products are normalised by taking a certain amount of liquid from each PCR output, either inversely proportional to their concentration, or fixed across PCRs. In the first (lysis buffer) normalisation step, the numerator (amount of lysis buffer taken for extraction) is fixed, while the denominator (total volume of lysis buffer) varies. In the second (PCR product) normalisation step, the numerator (amount of PCR liquid taken for sequencing) varies, while the denominator (total volume of PCR liquid) is fixed. It is standard procedure to record these normalisation

fractions, and in Section 2, we show how this information is incorporated into the model.

Generally, we should expect a positive relationship between the DNA biomass of a species in a sample and the count of reads obtained for that species in that sample (Luo et al., 2022), but this relationship is imperfect, due to noise and error (see Table 1). First, even given best practice, there are small but non-negligible probabilities (a) that a species' DNA in a sample fails to be amplified or sequenced, leading to false-negative error and (b) that a species' DNA cross-contaminates other samples and is amplified, leading to false-positive error (Stage 2 false negative and false positive errors are jointly referred to as *Stage 2 error*). We say that a PCR yields non-negligible reads for a species when the PCR product of that species is successfully read by the DNA sequencer (i.e. the PCR is successful), and otherwise, a PCR yields zero or non-zero but negligible reads, in which case we say that the PCR is not successful for that species. We note that a PCR can be successful, that is, yield non-negligible reads, not only when the biomass is present in the sample but also when it is not, in the latter case because of contamination. Additionally, PCR amplification also inevitably favours some species over others, due to PCR primer mismatch, resulting in species-specific amplification rates (*Stage 2 species effect*, equal within columns of the OTU table), and PCR and sequencing stochasticity results in different total numbers of reads across all species, even for the same sample (*Stage 2 pipeline effect*, equal within rows of the OTU table). Finally, due to the inherent stochasticity of the PCR and sequencing process, there is added noise in the resulting reads *in each cell* of the OTU table (*Stage 2 noise*).

In Stage 2, in addition to recording the normalisation fractions, different approaches are employed to understand and monitor some of the noise and error. One such approach is the so-called internal standard or *spike-in*, during which a known amount of DNA of a synthetic sequence or of a species that is known to be absent from all surveyed sites, is added to each sample. In addition, negative controls, which are samples that are known to not include DNA of any species, can be introduced in Stage 1 and Stage 2 (Ficetola et al.,

2015).

Table 1: Description of noise, error, and species/pipeline effects in the two stages of DNA-based surveys.

Stage 1 - DNA biomass collection	
Species effect	Every sample contains a certain amount of DNA biomass of each species, with the amount proportional to the DNA biomass available at the site. However, the proportionality constant is unknown and species-specific, since the DNA of different species can be collected at different rates.
Noise	The amount of DNA biomass collected for each species varies stochastically between samples collected at the same site and time.
Error	It is possible for the DNA of a target species that is present at a site not to be sampled (false negative error), or traces of DNA from one sample to contaminate another sample (false positive error).
Stage 2 - DNA biomass analysis	
Species effect	As a result of differences in gene copy number, DNA extraction efficiency, and PCR amplification efficiency, the correspondence between the source sample DNA biomass and the number of amplicon reads is species-specific (each column of the OTU table).
Pipeline effect	PCR stochasticity and the passing of small aliquots of liquid along the laboratory pipeline affects the total number of reads per technical replicate for all species (each row of the OTU table).
Noise	In addition to the species and pipeline effect, there is added noise in the number of reads per OTU and PCR (each cell of the OTU table).
Error	It is possible for the DNA of a target species that is present in the sample not to be amplified in the lab (false negative error), or traces of DNA of one sample to contaminate and be detected in other samples (false positive error), due to the high species-detection power of amplicon sequencing.

1.2 Existing approaches

A common approach for modelling metabarcoding data is to convert them to detection/non-detection data by thresholding the number of reads in the OTU table, with user-specified criteria. This allows the use of a generalized linear model (GLM) framework (Saine et al., 2020), which has also been extended to account for species correlation, for example using joint species distribution models (JSDMs) (Ovaskainen and Abrego, 2020). However, this approach does not account for the two stages or the noise and error inherent in DNA-based surveys (Table 1).

To that end, several different but related approaches have been proposed. A common approach applies occupancy models that account for false negative observation error to

the binary detection/no detection data (Ficetola et al., 2015). More recently, multi-scale extensions of these occupancy models have been proposed to account for false negative error in both stages (Mordecai et al., 2011; Schmidt et al., 2013) and for false positive error (Guillera-Arroita et al., 2017; Griffin et al., 2020) for a single species. However, the occupancy model framework disregards the information in the reads and relies on arbitrary thresholds about what constitutes a detection. Alternatively, the reads have also been modelled within a GLM framework (Takahara et al., 2012; Carraro et al., 2018) but without considering the errors in each stage. A joint model of species occupancy and corresponding reads was developed by Fukaya et al. (2022) but without considering the direct link between species DNA biomass at the site and species reads, or the correlation between species.

Finally, we note that an area of research similar to DNA-based biodiversity surveys is microbiome biology, which is the genetic material of all microbial life in an abiotic substrate (e.g. soil) or in a living host (e.g. the human microbiome). When modelling microbiome data, analysis has usually focused on understanding changes in the relative composition of each taxon across different samples. As a result, modelling approaches in this field have revolved around the Dirichlet-Multinomial, which allows inference of the changes, across samples, of the proportions of the species DNA biomasses(Fordyce et al., 2011; Coblentz et al., 2017; McLaren et al., 2019; Clausen and Willis, 2022), although within-species changes in DNA biomass are argued to be informative (Tkacz et al., 2018). A more detailed comparison between the model we introduce in this paper and models for microbiome data is given in Section 2.1.

1.3 Structure of the paper

In this paper, we present a unifying hierarchical modelling framework for OTU reads that considers key sources of variation, noise, and error at both stages of DNA-based biodiversity surveys (Table 1), while also modelling correlation between species and between sites. The model allows us to infer changes in DNA biomass and to link these changes to site-specific covariates.

We use state-of-the-art MCMC (Markov chain Monte Carlo) methods that build on recent work for hierarchical and crossed-effects models (Zanella and Roberts, 2021) as well as adaptive MCMC techniques (Andrieu and Thoms, 2008). In particular, we develop a novel sampling technique to improve mixing in the special case of a multivariate crossed-effect model with PCR-specific random effects, and we use adaptive updates of latent variables to focus sampling effort. This allows us to fit our model (with many latent variables across the different stages of DNA surveys) to data from large numbers of sites, samples per site, PCRs per sample, and species.

The new model, its properties, and links to existing models are presented in Section 2. Details on our approach to inference are given in Section 3. Issues of study design are explored and corresponding simulations are presented in Section 4. A case study of a large Malaise-trap metabarcoding dataset is presented in Section 5, and the paper closes with a discussion in Section 6.

2 Model

We assume that M_i physical samples are collected from site i, $i = 1, \ldots, n$, and K_{im} PCR replicates are performed on the m-th sample from site i. We denote by y^s_{imk} the number of DNA reads of the s-th species, $s = 1, \ldots, S$ in the k-th PCR replicate of the m-th sample collected at the i-th site. We have n_z site covariates and X^z_i represents their value at site i and n_w sample covariates, represented as X^w_{im} for the m sample at the i-th site. In what follows, i indexes sites, m samples, k PCR replicates, and s species.

Our proposed model (see Figure 2) is hierarchical, with three levels. The first level models the amount of DNA biomass of each species at the surveyed sites, which is a function of environmental and landscape covariates as well as between-species and between-sites correlation (**DNA biomass availability**). The second level models the amount of DNA biomass collected for each species in each physical sample from each site (**DNA biomass collection**). Lastly, the third level models the number of reads obtained for each species in each PCR from each physical sample (**DNA biomass analysis**). Data are

observed only at the third level, as the result of Stage 2 of the survey, with levels one and two corresponding to latent states.

DNA biomass availability $L = \{l_i^s\} \sim \text{MN}(B_0 + X_z B, \Sigma, T), \qquad T^{-1} \sim \text{GH}$

DNA biomass collection

$$\begin{gathered}\text{logit}(\theta_{im}^s) = \phi_0^s + \phi_1^s l_i^s + X_{im}^w \phi^s \\ \mathbb{P}(\delta_{im}^s = 1) = \theta_{im}^s, \\ \mathbb{P}(\gamma_{im}^s = 1 \mid \delta_{im}^s = 0) = \zeta^s,\end{gathered} \qquad v_{im}^s \sim \begin{cases} \text{N}(\eta_s + l_i^s + X_{im}^w \beta_s^W, \sigma_s^2) & \text{if } \delta_{im}^s = 1 \\ \text{N}(\mu_s, \nu_s^2) & \text{if } \delta_{im}^s = 0, \gamma_{im}^s = 1 \end{cases}$$

DNA biomass analysis

δ_{im}^s	γ_{im}^s	$\mathbb{P}(c_{imk}^s = x \mid \delta_{im}^s, \gamma_{im}^s)$ $x=0$	$x=1$	$x=2$
1	–	$1-p_s$	p_s	0
0	1	$1-p_s$	p_s	0
0	0	$1-q_s$	0	q_s

$$y_{imk}^s \sim \begin{cases} \pi\delta_0 + (1-\pi)(1 + \text{NB}(\mu_0, n_0)) & \text{if } c_{imk}^s = 0 \\ \begin{cases} \text{NB}(\exp(m_{imk}^s), r_s) \\ m_{imk}^s = \lambda_s + v_{im}^s + u_{imk} + o_{imk} \\ u_{imk} \sim \text{N}(0, \sigma_u^2) \end{cases} & \text{if } c_{imk}^s = 1 \\ \text{Pois}(\tilde{\mu}) & \text{if } c_{imk}^s = 2 \end{cases}$$

(a)

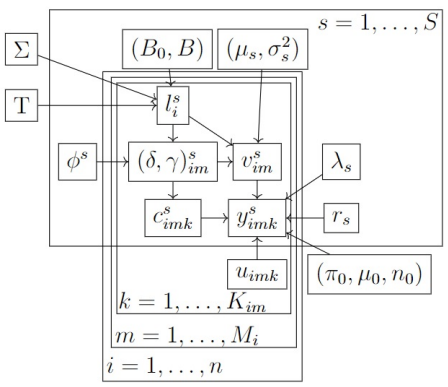

(b)

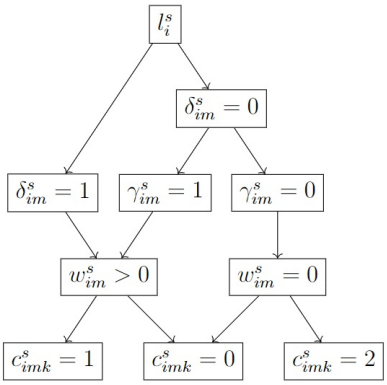

(c)

Figure 2: (a): Model summary, (b): Directed acyclic graph representing the relationships between the variables in the model. (c) Graphical representation of the latent indicator variables in the model.

DNA biomass availability We denote the logarithm of the amount of DNA biomass of species s in site i available for collection by l_i^s and denote the $n \times S$ matrix L by $\{L\}_{is} = l_i^s$. We model DNA biomass correlation between species and spatial correlation between sites by assuming that L follows a matrix normal distribution, $L \sim \text{MN}(B_0 + X^z B, \Sigma, T)$ (Dawid, 1981), where B_0 is an $n \times S$ matrix with columns $1_n \beta_0^s$, with β_0^s a species-specific intercept, X^z is a design matrix whose rows are X_i^z, B is an $n_z \times S$ matrix of regression coefficients, Σ is an $n \times n$ matrix modelling the correlation across sites, and T is an $S \times S$ matrix modelling the correlation across species. We note that, within this framework, the amount

of DNA biomass of a species at the surveyed site cannot be exactly 0, but can be negligible for modelling purposes as we describe below. We employ a graphical horseshoe (GH) prior (Li et al., 2019) for the inverse species covariance matrix $Q = T^{-1}$, which is defined by specifying the following *a priori* independent distributions on each element

$$Q_{ss} \propto \text{Exp}\left(\frac{\lambda}{2}\right),\ s = 1, \ldots, p, \quad Q_{ts} = Q_{st} \sim \text{N}(0, \lambda_{st}^2 \tau^2),\ \lambda_{st} \sim C^+(0,1), \quad s < t \leq S$$

subject to the constraint $T \in \Omega_S$, where Ω_S is the space of the positive definite $S \times S$ matrices, C^+ represents the half-Cauchy distribution (Gelman, 2006), and $\tau \sim C^+(0,1)$. Unlike Li et al. (2019) who specified a flat prior $Q_{ss} \propto 1$, we follow Wang (2012) and define a proper prior $Q_{ss} \sim \text{Exp}(\frac{\lambda_{GH}}{2})$, ensuring that T, which is latent, has a proper posterior. We model the spatial correlation matrix Σ using an exponential kernel function, so that $\Sigma_{i_1 i_2} = \sigma^2 \exp\left\{-\frac{(x_{i_1} - x_{i_2})^2}{l^2}\right\}$, where x_{i_1} and x_{i_2} are the locations of site i_1 and i_2, respectively. We note that we have accounted for species correlations in the DNA biomass availability stage, but any residual correlations of this type could also be the result of species correlations in the collection or analysis stages, discussed below. It is not possible, with metabarcoding data alone, to identify the source of these inferred correlations, and therefore, species correlations should be interpreted with caution.

DNA biomass collection We denote by w_{im}^s the amount of DNA biomass of species s collected in sample m from site i and $v_{im}^s := \log(w_{im}^s)$. To account for *Stage 1 false negative error* at this stage, we introduce the latent variable δ_{im}^s that is equal to 1 if DNA biomass for species i has been collected in the m-th physical sample from site i, and 0 otherwise. We assume that $\delta_{im}^s = 1$ with probability θ_{im}^s, which is a function of covariates X_{im}^w, and of l_i^s, since higher amounts of DNA biomass are expected to lead to a higher probability of collecting DNA biomass in the sample, leading to $\text{logit}(\theta_{im}^s) = \phi_0^s + \phi_1^s l_i^s + X_{im}^w \phi^s$. We note that as l_i^s tends to $-\infty$, θ_{im}^s tends to 0, and therefore the species becomes practically impossible to detect. If the amount of DNA biomass collected is greater than 0 ($\delta_{im}^s = 1$), we model $v_{im}^s \sim \text{N}(\eta_s + l_i^s + X_{im}^w \beta_s^w, \sigma_s^2)$, where η_s models *Stage 1 species effects* on the DNA biomass collection rate and σ_s^2 models the species-specific *Stage 1 noise* in the DNA

biomass collection rate. To account for *Stage 1 false positive error*, we introduce latent variable γ_{im}^s, which is equal to 1 with probability ζ^s if the collected DNA biomass is the result of contamination and 0 otherwise. We assume that γ_{im}^s can be 1 only if $\delta_{im}^s = 0$ and that $v_{im}^s \sim \mathrm{N}(\mu_s, \nu_s^2)$ if $\gamma_{im}^s = 1$. In this way, we assume that a sample which already contains DNA biomass of a species cannot be further contaminated by the DNA of the same species from another sample or site. We make this assumption as there is not enough information in the data to partition the collected DNA biomass between that which was truly collected from the site and that which was contamination from elsewhere.

DNA biomass analysis As mentioned above, by non-negligible reads we mean that some of the PCR product is successfully read by the DNA sequencer. We introduce latent variable c_{imk}^s to model the success of PCR k, sample m, and site i for species s, i.e. *Stage 2 error*. Firstly, if sample m from site i contains DNA biomass of species s ($w_{im}^s > 0$), PCR run k can be successful, i.e. non-negligible reads (true positive), $c_{imk}^s = 1$, or not successful, i.e. negligible reads (false negative), $c_{imk}^s = 0$, and we assume that $c_{imk}^s = 1$ with probability p_s. We note that we have assumed here that p_s only varies by species and not across sites or replicates in either stage. However, p_s could depend (negatively) on the total amount of DNA biomass in the sample, particularly in cases of low DNA concentration for that species or could vary across primers or between labs. We return to these issues in Section 6. Secondly, if sample m from site i does not contain DNA biomass of species s ($w_{im}^s = 0$), PCR run k can be successful if it yields non-negligible reads due to lab contamination (false positive), $c_{imk}^s = 2$, or not successful (again, $c_{imk}^s = 0$, true negative) and assume that $c_{imk}^s = 2$ with probability q_s.

We model the reads conditional on c_{imk}^s as follows. Conditional on $c_{imk}^s = 1$, $y_{imk}^s \sim \mathrm{NB}(\exp(\lambda_s + v_{im}^s + u_{imk} + o_{imk}), r_s)$, where λ_s models the *Stage 2 species effect* on the amplification rate, u_{imk} is the *Stage 2 pipeline effect*, with $u_{imk} \sim \mathrm{N}(0, \sigma_u^2)$, o_{imk} is an offset modeling the normalisation steps described in Section 1.1, and r_s is a species-specific variance of the *Stage 2 noise*. If more than one normalisation step is employed, then

they can all be incorporated into the same offset as a sum. Conditional on $c^s_{imk} = 0$, $y^s_{imk} \sim \pi\delta_0 + (1-\pi)(1 + \text{NB}(\mu_0, n_0))$, that is, there are zero reads with probability π, and non-zero but negligible reads otherwise. Finally, conditional on $c^s_{imk} = 2$, $y^s_{imk} \sim \text{Pois}(\tilde{\mu}_s)$. The negative binomial is parameterised in terms of the mean and the number of failures. A visual representation of the PCR process when $c^s_{imk} = 1$ is shown in Figure 1 of the Supplementary material.

Stage 2 negative control samples (which are known to not contain DNA of any species) can be easily accounted for in our model by having additional samples for which $\tilde{\delta}^s_l = \tilde{\gamma}^s_l = 0$. Accounting for spike-ins corresponds to having $S^\star$ additional species for which $(v^{S+1}_{im}, \ldots, v^{S+S^\star}_{im})$ is known. Since the pipeline effect is shared across all species (including spike-ins), the known values of v^s_{im} for the spike-ins help to better estimate u_{imk}. We further investigate this effect in Section 4.

The model is summarised in Figure 2 (a), the directed acyclic graph of the model is shown in Figure 2 (b), while a graphical representation of the latent variables introduced across both stages is shown in Figure 2 (c). The model allows both zero-inflation and overdispersion (even after accounting for zero-inflation) of the reads. In the case of true positives (when $c^s_{imk} = 1$), we allow overdispersion through the negative binomial distribution and the introduction of the offset. The use of negative binomial is a standard choice for overdispersed data, particularly in Bayesian modelling. Ver Hoef and Boveng (2007) discuss the merits of negative binomial and quasi-Poisson regression modelling in ecological data. Datta and Dunson (2016) discuss how a scale mixture of negative-binomial regression models can be used for so-called quasi-sparse counts, which are often small, not zero.

The model presented in Figure 2 is not identifiable in its general form unless certain constraints are applied, as we discuss below. For example, choosing for simplicity Σ and T to be diagonal, if we define $\tilde{v}^s_{im} := v^s_{im} - \eta_s - l^s_i$ and $\tilde{l}^s_i := l^s_i - \beta^s_0$, the model for θ^s_{im} and y^s_{imk} conditional on $c^s_{imk} = 1$ and all offsets o_{imk} set to 0 can be expressed as

$$\begin{cases} \tilde{l}_i^s \sim \mathrm{N}(X_i\beta_s^z, \tau_s^2) \\ \tilde{v}_{im}^s \sim \mathrm{N}(X_{im}\beta_s^w, \sigma_s^2) \\ \theta_{im}^s = \mathrm{logit}(\phi_0^s + \phi_1^s\beta_0^s + \phi_1^s\tilde{l}_i^s + \phi^s X_{im}^s) \\ y_{imk}^s \sim \mathrm{NB}\left(\exp(\beta_0^s + \tilde{l}_i^s + \eta_s + \tilde{v}_{im}^s + \lambda_s + u_{imk}), r_s\right) \end{cases} \tag{1}$$

It is evident that the model is invariant to transformations of the form

$$(\beta_0^s)^\star = \beta_0^s + c + d, \quad (\lambda_s)^\star = \lambda_s - c, \quad (\eta_s)^\star = \eta_s - d, \quad (\phi_0^s)^\star = \phi_0^s - \phi_1^s(c+d).$$

The reason for this unidentifiability is that data are observed only in the third level of the model, and hence the following sets of species-specific parameters are confounded: the baseline amount of DNA biomass across all sites (β_0^s) with the baseline collection rate (η_s) and the baseline amplification rate (λ_s), and the former again with the baseline detection rate ϕ_0^s. However, by assuming that all these baseline rates are constant across sites, samples, and PCRs, we are able to infer species-specific *changes* in DNA biomass across sites and therefore covariate effects.

For inferential purposes, we reparameterise the model and set the new baseline (log) amount of DNA biomass, $(\beta_0^s)^\star$, equal to $\beta_0^s + \eta_s$, which means that we can only estimate the sum of the baseline amount of available DNA biomass and the corresponding baseline collection rate for the same species. Similarly, we set the new baseline (logit) collection probability $(\phi_0^s)^\star$, equal to $\phi_0^s - \phi_1^s\eta_s$, since the baseline collection probability is also confounded with the baseline collection rate (equivalent to setting $\phi_0^s \equiv 0$ and $\eta_s \equiv 0$ in Equation (1)).

As a result, we cannot infer the amount of available DNA biomass separately from the collection rate, and hence the estimates of log DNA biomass obtained, as mentioned above, are only meaningful for comparison *within* each species. For the same reason, comparisons of absolute amount of DNA biomass *across* species are not meaningful. We also note that depending on the survey design in terms of the number of samples collected per site and the number of PCR replicates per sample, additional sets of parameters can be confounded and not estimable. Specifically, the following pairs of parameters are confounded:

- $S = 1$: pipeline effect u_{imk} and PCR variance r_s,

- $K = 1$: PCR variance r_s and sample noise $\tilde{v}^s_{im}$,
- $M = 1$: sample noise $\tilde{v}^s_{im}$ and site noise $\tilde{l}^s_i$.

These are pathological cases that arise when there is no replication at the site/sample/PCR levels. Replication is vital for being able to account for and to estimate the effects of the different sources of noise and error (Buxton et al., 2021), an issue to which we return in Section 4.1. Finally, we note that if the offsets o_{imk} introduced in the model due to the several normalisations occurring in the pipeline are not recorded, the link between the amount of DNA biomass in the environment and the reads is broken. However, a potential way to restore this link is the introduction of spike-ins, which contribute to the estimation of the "overall" pipeline effects $\tilde{u}_{imk} = u_{imk} + o_{imk}$.

2.1 Special cases

Two models available in the literature (Section 1.2) arise as special cases of our model. First, the Dirichlet-Multinomial model (DMM) (Fordyce et al., 2011) is expressed through the following hierarchy (omitting the indexes m and k to simplify notation):

$$\begin{cases} (y^1_i, \dots, y^S_i) \sim \text{Multi}(N_i, \pi^1_i, \dots, \pi^S_i) \\ (\pi^1_i, \dots, \pi^S_i) \sim \text{Dirichlet}(w\alpha^1, \dots, w\alpha^S) \end{cases} . \tag{2}$$

where $N_i = \sum_{s=1}^S y^s_i$. The DMM can be seen as a special case of the model described in Section 2, for the Stage 2 process, conditional on $\delta^s_i = 1$. Specifically, $y^s_i \sim \text{NB}(\exp(\lambda_s + v^s_i + u_i), r_s)$, and therefore, assuming $\lambda_s = u_i = 0$, if $r_s \to \infty$, the distribution for y^s_i converges to a $\text{Pois}(\exp(v^s_i))$. Conditional on N_i, the model is a $\text{Multi}\left(N_i, \pi^1_i, \dots, \pi^S_i\right)$, where $\left(\pi^1_i, \dots, \pi^S_i\right) = \left(\frac{\exp(v^1_i)}{\sum_s \exp(v^s_i)}, \dots, \frac{\exp(v^S_i)}{\sum_s \exp(v^s_i)}\right)$. Next, assuming $\exp(v^s_i) \sim \text{Gamma}(w\alpha_s, \theta)$, we obtain $(\pi^1_i, \dots, \pi^S_i) \sim \text{Dirichlet}(w\alpha_1, \dots, w\alpha_S)$. Finally, as the DMM does not take errors into account, the equivalence with our model can be obtained by setting $p_s \equiv 1$.

McLaren et al. (2019) propose to account for the Stage 2 species effect in the DMM framework by modelling the probabilities $(\pi^1_i, \dots, \pi^S_i)$ as $(\frac{e^1\tilde{\pi}^1_i}{\sum_s e^s\tilde{\pi}^s_i}, \dots, \frac{e^S\tilde{\pi}^S_i}{\sum_s e^s\tilde{\pi}^s_i})$, where e_s models the species-specific efficiencies, which in our model is achieved by using a species-specific λ_s. The DMM can be extended hierarchically if nested treatments are considered

(Coblentz et al., 2017) by defining a nested prior $(\alpha^1, \ldots, \alpha^S) \sim \text{Dirichlet}(\alpha_0^1, \ldots, \alpha_0^S)$ for each level. In our model, this is achieved by a hierarchy of normal priors. This highlights a key difference between the DMM approach and the approach we introduce in this paper, since we model the propagation of the *absolute* amount of DNA biomass across the different stages, while the DMM models the propagation of the *relative* amount of DNA biomass.

Secondly, the occupancy model of Griffin et al. (2020), in the simple case of no covariates,

$$\begin{cases} z_i \sim \text{Be}(\psi) \\ w_{im} \sim \text{Be}(z_i\xi_1 + (1 - z_i)\xi_0) \\ y_{imk} \sim \text{Be}(w_{im}p + (1 - w_{im})q) \end{cases} \tag{3}$$

designed for (single-species) qPCR, can be seen as a special case of our model when the information in the counts is not considered. Specifically, letting l_i be binary, with $l_i \in \{-\infty, 0\}$, and defining $z_i = \exp(l_i)$, we obtain $\theta_{im}|(l_i = -\infty) = 0$ and $\theta_{im}|(l_i = 0) = \text{logit}(\phi_0)$. Hence, the model for δ and c becomes

$$\begin{cases} \delta_{im} \sim \text{Be}(z_i(\text{logit}(\phi_0) + (1 - \text{logit}(\phi_0))\zeta) + (1 - z_i)\zeta) \\ c_{imk} \sim \text{Be}(\delta_{im}p + (1 - \delta_{im})q) \end{cases},$$

which is identical to the Griffin et al. (2020) model after defining $\xi_1 = \text{logit}(\phi_0) + (1 - \text{logit}(\phi_0))\zeta$ and $\xi_0 = \zeta$.

3 Inference

Samples can be drawn from the posterior distribution of the parameters using a Gibbs sampler. Posterior sampling is greatly helped by representing the negative binomial distribution as a Gamma-Poisson mixture, which allows many parameters to be updated in closed form from their full conditional distribution.

For the parameters σ_s, μ_s, B and B_0, the full conditional distribution is available in closed form, and therefore posterior sampling is straightforward. We use simple random walk Metropolis-Hastings steps for parameters π, μ_0, n_0, and r_s and Metropolis-Hastings steps with a Laplace approximation proposal for the parameters l_i^s, λ_s, v_{im}^s, u_{imk} and r_s. However, on its own, this naive Gibbs sampler will mix slowly since we have a complex hierarchical model with crossed-effects and many latent variables. We address this by

updating parameters in blocks using re-parameterisation and an adaptive updating scheme for the discrete latent variables.

To illustrate our approach to blocking and re-parameterisation, we consider the error-free version of our model

$$\begin{cases} l_i^s \sim \mathrm{N}(0, \tau_s^2) \\ v_{im}^s \sim \mathrm{N}(l_i^s, \sigma_s^2) \\ u_{imk} \sim \mathrm{N}(0, \sigma_u^2) \\ y_{imk}^s \sim \mathrm{NB}(\exp(\lambda_s + v_{im}^s + u_{imk}), r_s) \end{cases} \tag{4}$$

A naive Gibbs sampler updating each parameter from its full conditional leads to prohibitively slow mixing, due to the form of the likelihood where λ_s, v_{im}^s and u_{imk} appear as a sum. To address the slow mixing in the nested effects, λ_s and v_{im}^s, the use of a centred parameterisation (Papaspiliopoulos et al., 2007) has been suggested, which corresponds to defining $\bar{v}_{im}^s := \lambda_s + v_{im}^s$ and $\bar{l}_i^s := \lambda_s + l_i^s$. However, issues of slow mixing still exist between $\bar{v}_{im}^s$ and u_{imk} and, as noted by Zanella and Roberts (2021), re-parameterisation does not improve mixing in the case of crossed-effects models. In a classic crossed-effect model of the form $y_{jkl} \sim \mathrm{N}(\lambda + v_j + u_k, \sigma^2)$, Papaspiliopoulos et al. (2020) propose a collapsed Gibbs sampler by first jointly sampling λ with v_j and then λ jointly with u_k. However, this approach does not scale well in our setup, since it would involve sampling all the λ_s and u_{imk} jointly, which have dimensions S and the total number of PCR technical replicates $\sum_{i,m} K_{im}$ respectively. Zanella and Roberts (2021) propose the use of identifiability constraints on the model, which in Equation (4) correspond to assuming $\sum_s v_{im}^s = \sum_k u_{imk} = 0$. Since sampling conditionally on constraints can be challenging, we propose a simpler strategy to improve mixing that is more suited to our framework. We consider re-parameterising to the *factor averages* $\hat{v}_{im} = \frac{1}{S}\sum_{s=1}^{S} \bar{v}_{im}^s$ and $\hat{u}_{im} = \frac{1}{K}\sum_{k=1}^{K} u_{imk}$ and the *factor increments* $\tilde{v}_{im}^s = \bar{v}_{im}^s - \hat{v}_{im}$ and $\tilde{u}_{imk} = u_{imk} - \hat{u}_{im}$ and performing an update by first sampling jointly the factor means conditional on the increments, that is, from $(\hat{v}_{im}, \hat{u}_{im} | \tilde{v}_{im}^s, \tilde{u}_{imk})$ and next using the standard updates $(u_{imk} | v_{im}^1, \ldots, v_{im}^S)$ and $(v_{im}^j | u_{im1}, \ldots, u_{imK})$. In our simulations, we have found that jointly updating the factor means considerably improves mixing.

The sampling scheme for the complete model is presented in the Supplementary material.

The indicator variables $(\delta^s_{im}, \gamma^s_{im}, c^s_{imk})$ can be updated directly from their full conditional distributions but, since there are $nMS(\bar{K}+2)$ (where $\bar{K}$ is the average number of PCR replicates) of these variables and often one value of $(\delta_{imk}, \gamma_{imk}, c_{imk})$ has probability very close to 1, evaluating every full conditional distribution in every iteration can be very time-consuming and computationally wasteful. Therefore, we use a cheap approximation as a proposal in a Metropolis-Hastings step. Specifically, every B iterations, we update the approximation $\hat{p}((\delta^s_{im}, \gamma^s_{im}, c^s_{imk}) = (\epsilon_1, \epsilon_2, \epsilon_3)) = \frac{1}{T}\sum_{t=1}^{T} \mathrm{I}\left((\delta^s_{im})^{(t)}, (\gamma^s_{im})^{(t)}, (c^s_{imk})^{(t)}) = (\epsilon_1, \epsilon_2, \epsilon_3)\right)$, where $(\delta^s_{im})^{(t)}, (\gamma^s_{im})^{(t)}, (c^s_{imk})^{(t)}$ is the value of $(\delta^s_{im}, \gamma^s_{im} c^s_{imk})$ at the t-th iteration, $\mathrm{I}(A)$ is the indicator function, which takes the value 1 if A is true and 0 otherwise, and T is the number of current iterations. Using this update scheme, we only need to evaluate the likelihood if the state is proposed to change. If the probability of one state is close to one, the adaptive scheme often proposes the current state, which can be accepted without computation. The adaptive scheme does not affect convergence of the MCMC algorithm since the approximation clearly has diminishing adaptation, and the state space of the indicator variables is discrete (see *e.g.* Roberts and Rosenthal, 2009, for more discussion of conditions for convergence of adaptive MCMC schemes).

4 Study design

In this section, we use a simplified version of the model to investigate the properties of our modelling approach under different study designs in terms of the number of sites, samples per site, and PCRs per sample, as well as the number of spike-ins. In each section, we consider the estimates of the differences in log DNA biomass, when log DNA biomass is not a function of site-specific covariates (no covariate case), and the estimates of the covariate coefficients when log DNA biomass is a function of a single continuous covariate (regression case). In Section 4.1 we present theoretical results using a continuous version of our model that does not account for error in either stage. In Section 4.2 we fit our model as presented in Section 2 under different scenarios for study design by varying the number

of sites, number of samples per site, and number of PCRs per sample. Finally, in Section 4.3, we explore the effect of spike-ins for different levels of noise in each stage of the process and different study designs.

4.1 Theoretical results for a simplified version of the model

We consider a normal approximation of the model presented in Section 2, which assumes no species or site correlations, that both stages are error-free by setting $\theta_{im}^s = p_s = 1$, and that the variances of the distributions of the noise at each stage are the same across species. As mentioned in Section 2, the use of spike-ins corresponds to the presence of species in the sample for which $(v_{im}^{S+1}, \ldots, v_{im}^{S+S^\star})$ is known. We assume, without loss of generality, that $v_{im}^{S+j} = 0$ for $j = 1, \ldots, S^\star$. We have the following proposition.

Proposition 4.1. *Consider the model* $\lambda_s \sim N(0, \sigma_\lambda^2)$ *for* $s = 1, \ldots, S + S^\star$ *and, for* $i = 1, \ldots, n$, $k = 1, \ldots, K$, $m = 1, \ldots, M$,

$$u_{imk} \sim N(0, \sigma_u^2), \qquad v_{im}^s \begin{cases} \sim N(l_i^s, \sigma^2), & s = 1, \ldots, S \\ = 0, & s = S+1, \ldots, S+S^\star \end{cases},$$

$$y_{imk}^s \sim N(u_{imk} + \lambda_s + v_{im}^s, \sigma_y^2), \quad s = 1, \ldots, S + S^\star$$

where σ^2, σ_u^2 *and* σ_y^2 *are known.*

(a) If we assume $p(l_i^s) \propto 1$ *and* $\sigma_\lambda^2 \in (0, \infty)$ *is known, then*

$$\mathrm{Var}(l_1^s - l_2^s | y) = \frac{1}{M}\left(\sigma^2 + \frac{\sigma_y^2}{K}\left(1 + \frac{\frac{\sigma_u^2}{\sigma_y^2}}{\frac{\sigma_u^2}{\sigma_y^2}S^\star + 1}\right)\right). \tag{5}$$

(b) If we observe a single covariate $X_i \overset{i.i.d.}{\sim} N(0, 1)$ *for the i-th site and assume* $l_i^s \sim N(X_i\beta_s, \tau^2)$ *with* $\sigma_\lambda^2 = \infty$ *(i.e.* $p(\lambda_s) \propto 1$*) and* $p(\beta_s) \propto 1$, *then*

$$\mathrm{Var}(\beta_s | y) = \frac{1}{n-1}\left(\tau^2 + \frac{1}{M}\left(\sigma^2 + \frac{\sigma_y^2}{K}\right)\right) \times (1 + C) \tag{6}$$

where $C = \frac{\sigma_u^2}{\sigma_y^2 + (M\tau^2 + \sigma^2)K(1 + S^\star \frac{\sigma_u^2}{\sigma_y^2}) + \sigma_u^2(S + S^\star - 1)}$.

Here σ_y^2 models the variance of the noise in Stage 2, as was the case for r_s in the original model. Equations (5) and (6) show the contributions of the variances at each stage to the posterior variance of the corresponding estimates (changes in biomass between sites, on the log scale, and covariate coefficients, respectively) in this special case.

The results for this special case suggest that, for both $\text{Var}(l_1^s - l_2^s|y)$ and $\text{Var}(\beta|y)$, increasing replication at a given stage decreases the contribution of the error variance at that stage and all downstream stages. For example, increasing the number of samples M per site reduces the contribution of the noise variance σ^2 at Stage 1 and at all downstream stages, i.e. σ_y^2 and σ_u^2 in Stage 2. Whereas, increasing the number of PCR replicates, K, only reduces the contribution of the Stage 2 variances (σ_u^2 and σ_y^2). Additionally, the benefit of the spike-in is greater as the ratio of variances $\frac{\sigma_u^2}{\sigma_y^2}$ increases. Moreover, in the case of $\text{Var}(\beta|y)$, if σ^2 is much greater than σ_y^2, the benefit of the spike-in is negligible, as the noise induced by σ^2 greatly outweighs the noise that can be mitigated via the use of spike-ins.

4.2 Simulated results for the full model; varying n, M, and K

We turn our attention to the full model in Fig. 2 and again consider two cases: no covariates and a single covariate, $X_i \sim \text{N}(0, 1)$. In the no covariate case, we consider the model's ability to estimate the correct sign of the difference of species log DNA biomasses at two sites. We use the Brier score $b(i_1, i_2, s) := (\bar{p}(l_{i_1}^s > l_{i_2}^s) - \delta_{i_1,i_2})^2$, where $\bar{p}(l_{i_1}^s > l_{i_2}^s)$ is the posterior probability of $l_{i_1}^s > l_{i_2}^s$ and δ_{i_1,i_2} is 1 if the true value of $l_{i_1}^s$ is greater than the true value of $l_{i_2}^s$ and 0 otherwise. We generate $l_i^s \sim \begin{cases} \text{N}(1, \tau_s^2) & i \text{ odd} \\ \text{N}(0, \tau_s^2) & i \text{ even} \end{cases}$ which separates the sites between those with "high" DNA biomass and those with "low" DNA biomass. We use $S = 40$ species, $n = 300$ sites, $M \in \{1, 2, 3, 4, 5\}$ samples per site and $K \in \{1, 2, 3, 4\}$ PCR replicates. The values of the other parameters are reported in the Supplementary Material. We have performed 50 replications for each combination of values of the design parameters, M and K. We report the average $b(i_1, i_2, j)$ spanning i_1 across the sites with low DNA biomass, i_2 across the sites with high DNA biomass, and s across all species

and across the replicates. As expected, the Brier score decreases, and hence the ability to distinguish between sites with low and high DNA biomass increases, as M and K increase (Figure 3). However, the benefit of increasing K decreases with M, which highlights the greater importance of multiple sample replicates per site in Stage 1.

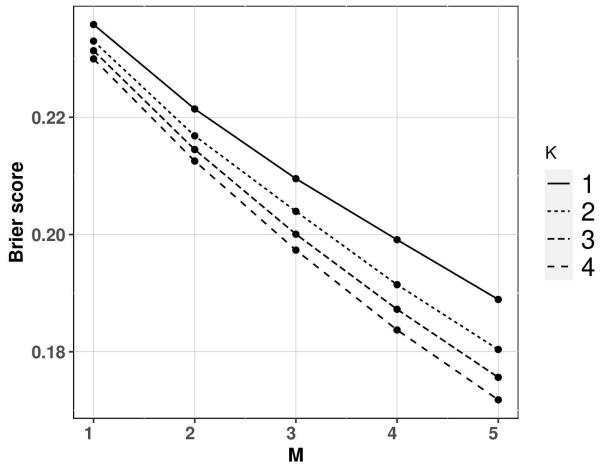

Figure 3: Brier score for distinguishing high and low DNA biomass sites, as a function of the number of samples (M) and number of PCR replicates (K). We have only considered $M \leq 5$, since greater M is unrealistic, and set $n = 300$.

In the regression case, we consider the absolute error and posterior standard deviation of the covariate coefficient β_s. We use $n \in \{50, 100, 200\}$ sites, $M \in \{1, 2, 3\}$ samples per site and $K \in \{1, 2, 3\}$ PCR replicates per sample and $S = 40$ species. The values of the other parameters are reported in the Supplementary Material. We performed 50 replicates for each combination of values of the design parameters and averaged results across all replicates and species. Results are shown in Figure 4.

As expected, absolute error and posterior standard error both decrease with more sites n, samples per site M, and PCRs per sample K. Doubling the number of sites from 50 to 100 has a bigger effect than doubling them again from 100 to 200, suggesting that the benefit of increasing the number of sampled sites decreases as the number of sites gets large. Collecting two samples per site instead of one drastically decreases both absolute error and posterior standard deviation, whereas the effect is less pronounced when the number of samples is further increased to three compared to two, and the same can be said about the number of PCRs.

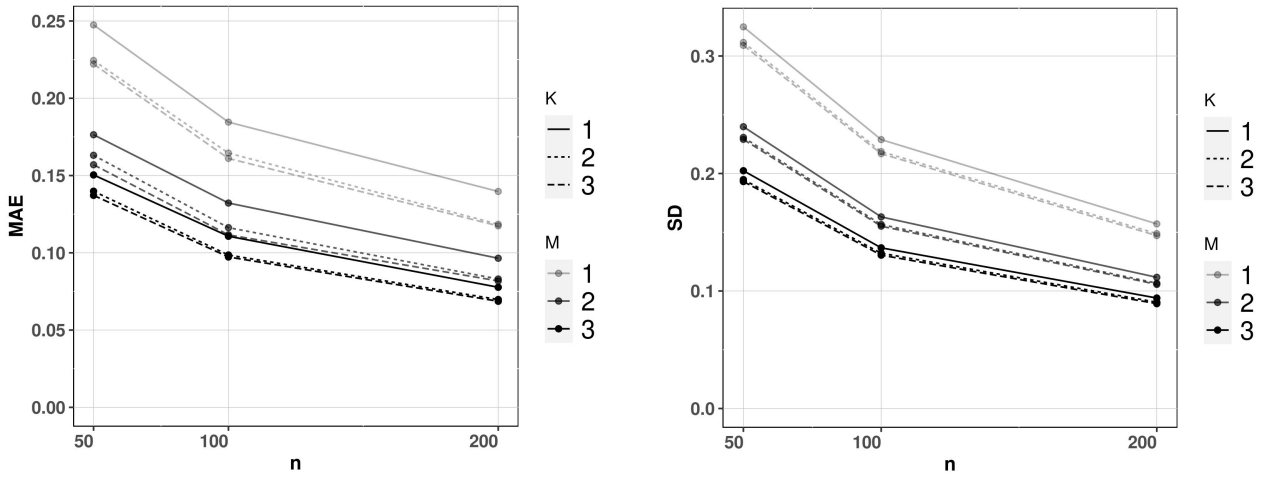

(a) **(b)**

Figure 4: Mean absolute error, (a), and posterior standard deviation, (b), averaged across all species and all simulations, of the covariate coefficient β^s for varying numbers of sites (n), samples per site (M), and numbers of PCR replicates per sample (K).

4.3 Spike-ins

In this section, we consider the improvement in inference when $S^\star$ spike-ins are employed in Stage 2. The effect of the spike-ins is maximised in the case of no false negative/positive errors, otherwise the benefit of the spike-ins is lower, and dependent upon the level of error. Therefore, in this section we consider data and corresponding model with no false positive/negative errors.

We simulated data on $n = 300$ sites, $M \in \{1, 2, 3\}$ samples per site, and $K \in \{1, 3\}$ PCR replicates per sample on $S = 10$ species. For each setting of M and K, we have fitted the model when $S^\star \in \{0, 1, 2, 3\}$ and report in each case the posterior relative error and posterior relative variance of the estimates, which are calculated by dividing the posterior error/variance by the corresponding error/variance when using $S^\star = 0$ (which is the case with the greatest error/variance).

Results of the simulation study are presented in Figure 5. In both cases, improvements diminish for $S^\star \geq 2$, and in most cases $S^\star = 1$ already provides most of the improvement, suggesting that the benefit of more than one spike-ins is minimal. The no covariate case is shown in the first row of Figure 5. Spike-ins contribute more to reducing biomass-change estimation error and variance with $M > 1$, with $M = 1$ resulting in virtually no

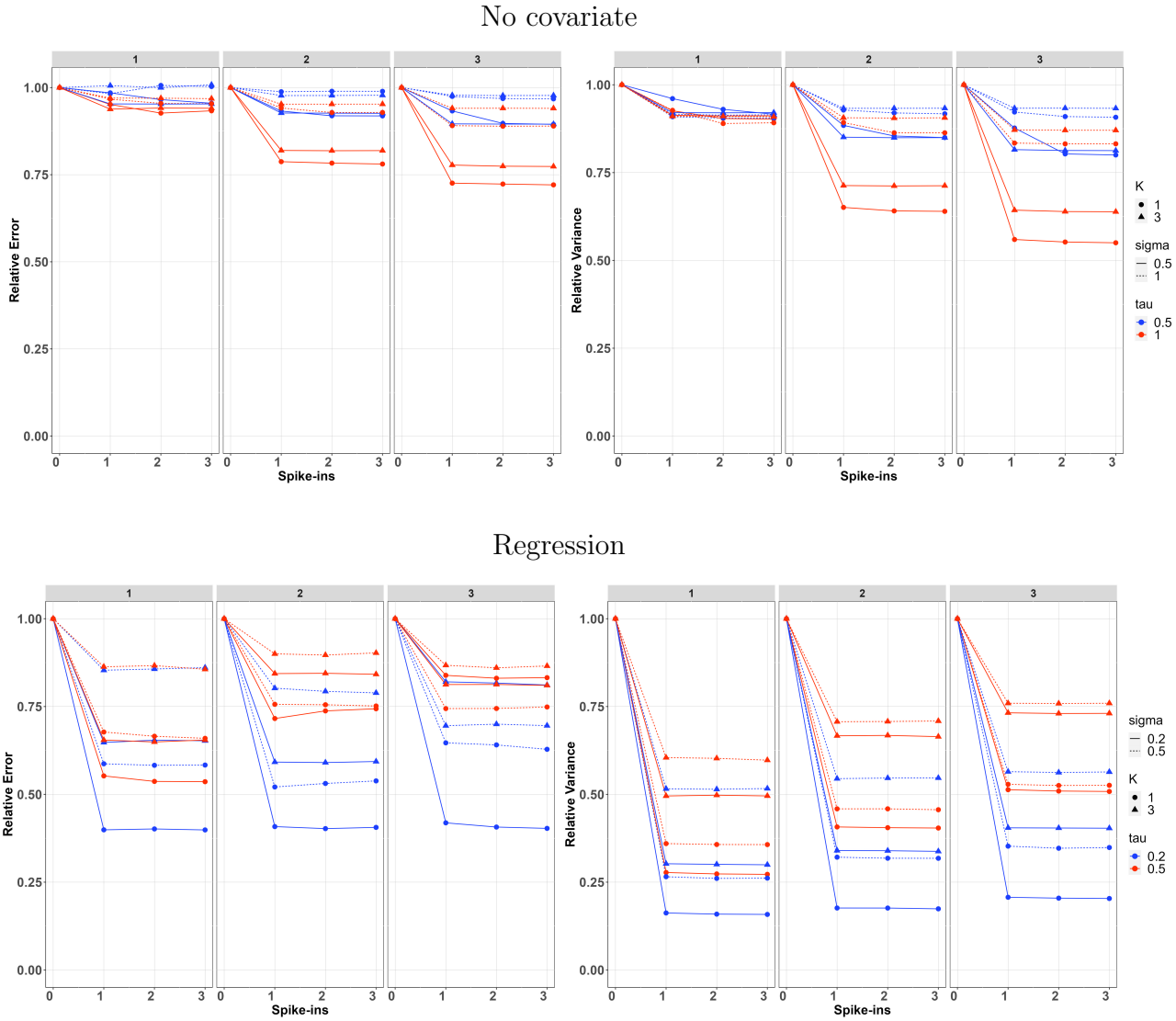

Figure 5: Effect of spike-ins on inference. The three facets per figure represent simulations with $M = 1/2/3$ samples per site. The between-samples standard deviation, σ, is represented by the line type, the between-sites standard deviation, τ, is represented by the color, the number of PCR replicates, K, is represented by the symbols. The first column represents the posterior relative error of the estimates and the second column represents the posterior relative variance.

improvements for any setting considered in the simulation. When $M > 1$, improvement is more pronounced when $K = 1$ instead of $K = 3$, because in the latter case, thanks to this replication at Stage 2, there is already increased information for estimating the pipeline effect. This is particularly true when τ is 1 instead of 0.5, because in this case, the differences between sites are more pronounced. For both values of τ, improvements are bigger when the between-samples standard deviation (σ) is smaller, since otherwise, Stage 1 noise dominates the process and understanding noise in Stage 2 decreases the overall

variance proportionally less.

The second row of Figure 5 shows the regression case. We have chosen smaller values for σ and τ (.2 and .5), since the relative contribution of the spike-ins is negligible with larger values. Spike-ins contribute more to reducing error and variance when the between-samples standard deviation (σ) and the between-sites standard deviation (τ) is smaller because, similar to before, the noise at early stages dominates the process, and therefore the relative contribution of the spike-ins is smaller. Also similar to the no covariate case, the contribution of the spike-ins is higher for $K = 1$ PCR replicates compared to $K = 3$. However, unlike that case, the contribution does not appear to increase as the number of samples per site M increases.

5 Case study

We apply our model to an unpublished amplicon sequencing dataset of arthropod invertebrates collected using 121 Malaise-trap samples from 89 sample sites in the H.J. Andrews Experimental Forest (HJA), Oregon, USA (225 km^2) in July 2018 (site details are provided in Li et al. 2024). Each trap was left to collect for seven days, and samples were transferred to fresh 100% ethanol to store at room temperature until extraction. The management objective that motivated the collection of this dataset is to interpolate continuous species distributions among the 89 sample points so that areas of higher and lower conservation value at the HJA can be identified.

For each sample, the collected invertebrate samples were combined with a lysis buffer, in an amount proportional to the starting sample mass, to digest the tissue, and a fixed aliquot was then taken from the overall mixture (and recorded) for DNA extraction and subsequent three PCRs. This normalization, as described in Section 2, was accounted for in the model by setting the offset o_{imk} equal to the log ratio between the aliquot and the overall amount of liquid mixture in each case. We included 50 species in the study by selecting the species that have the most non-zero counts across all PCR replicates. Log DNA biomass is modelled as a function of two environmental covariates: log elevation and

log distance-to-road.

Figure 6 presents the 95% posterior credible intervals (PCIs) for the species-specific coefficients of log elevation and log distance-to-road in the model for log DNA biomass. The effects of the covariates on species DNA biomass are not consistent within each taxonomic order, which suggests low phylogenetic inertia at this rank for response to these landscape characteristics. Elevation is a stronger predictor for species DNA biomass than distance-to-road for this ecosystem. This makes ecological sense, since distance-to-road is only expected to exert an effect over about 100 meters, via canopy openness, whereas elevation exerts a pervasive effect via its effects on temperature, precipitation, and vegetation.

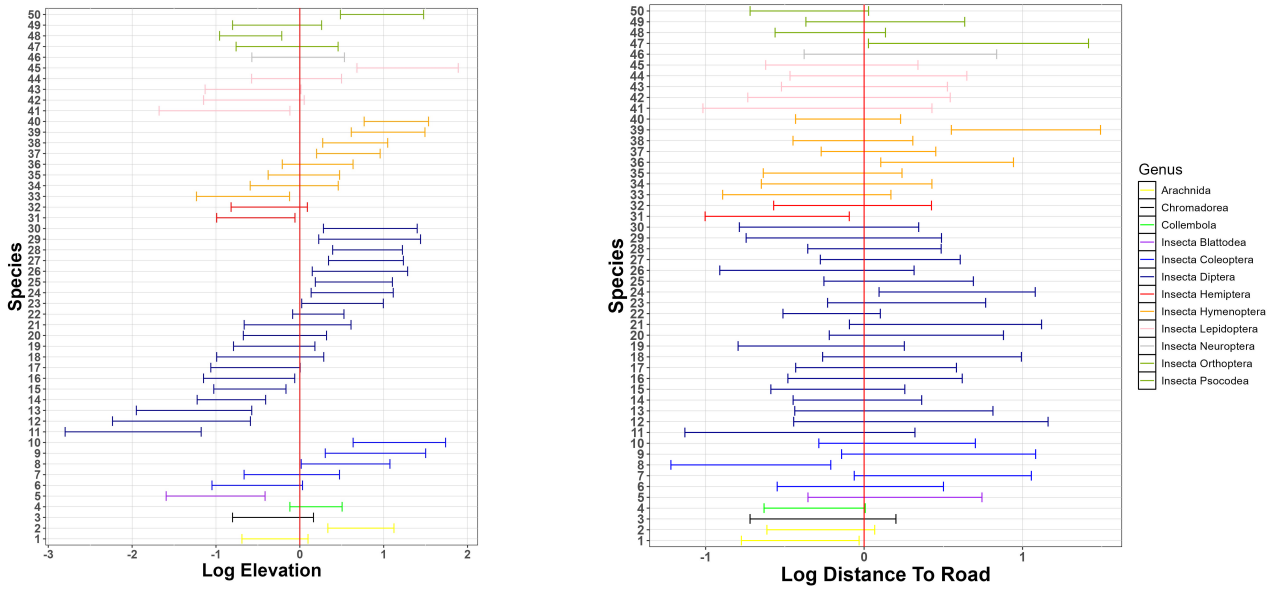

Figure 6: Case study: 95% PCI of the species-specific coefficients of log elevation (left) and distance to road (right) in the model for log DNA biomass. Species are grouped taxonomically.

Figure 7 (a) presents the posterior mean of the between-species residual correlations. We set $\lambda_{GH} = 1$ in the GH prior and we emphasize that the GH prior assumes no prior structure imposed on the taxa. Species in the Diptera (flies, spp. 14-30) exhibit higher positive correlations with each other, as well as with several species in the Hymenoptera (ants, bees, and wasps) and Lepidoptera (butterflies and months). We conservatively interpret these positive residual correlations as indicative of unmeasured environmental covariates, such as canopy openness, rather than of biotic interactions. We also note that two species in

the Lepidoptera, (spp. 41, 43), one in the Hymenoptera (sp. 33), and one in the Psocodea (barklice, sp. 50) are among the few species showing strong negative residual correlation with many of the other species, and again, we conservatively interpret these correlations as indicative of unmeasured environmental covariates. There is a strongly positive, pairwise correlation between two tabanid fly species *Hybomitra liorhina* and *Hybomitra* sp. (spp. 12, 13), which might indicate the oversplitting of one biological species into two OTUs during the bioinformatic pipeline. Finally, there is also a strongly positive, pairwise correlation between the moth species *Ceratodelia gueneata* (sp. 44) and the predatory fly (Scathophagidae, *Microprosopa* sp., (sp. 20), which might indeed indicate a specialised predator-prey relationship. All that said, we highlight that these inferred correlations have been accounted for in the DNA availability stage of the model, but, as we discuss in Section 2, they can also be the result of the DNA biomass collection or analysis stages, so should be interpreted with caution.

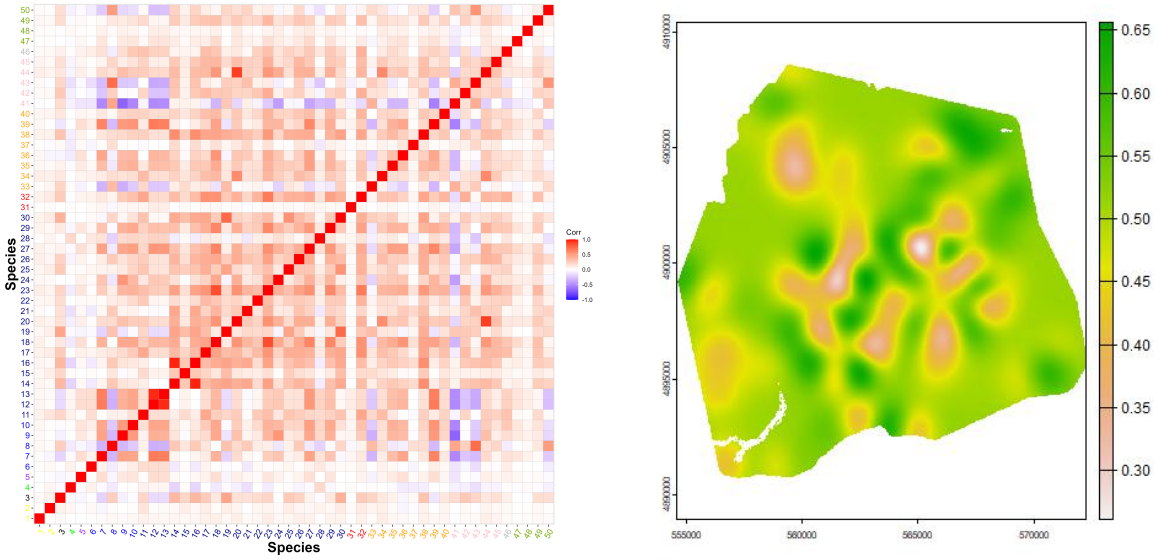

Figure 7: Case study. Left: Correlation plot of all species. Red represents positive correlations while blue represents negative correlations. Species are grouped taxonomically. Right: Posterior mean of biomass-weighted species richness across the study area. For each species, we rescale the log-biomass amount across all study sites into the range $[0, 1]$ and next we compute the species richness as the sum of all the rescaled biomasses across all species.

In Figure 7 (b), we show the biodiversity map for the area, which is useful for identifying areas of higher species richness and compositional distinctiveness, which together can be

used to identify areas of higher conservation value (i.e. higher 'site irreplaceability' *sensu* Baisero et al., 2022). The predicted mean log DNA biomasses on a continuous map over the HJA for all individual species are presented in the Supplementary Material. These can be used to identify species with a wide spatial range, such as the click beetle (*Megapenthes caprella*), or with a restricted range, such as the leafhopper (*Osbornellus borealis*).

Finally, Figure 8 (a) suggests that generally, there is a similar amount of variation between sites and between samples for these species. As suggested by Figure 8 (b), the species that we have considered have similar collection probabilities across the several sites, possibly due to the fact that the most frequently detected species across PCRs have been selected. Figure 8 (c) demonstrates, as expected, that the Stage 2 true positive probability is close to 1 for all species. We highlight here that this probability is modelled as species-specific but assumed constant across all replicates. Similarly, the figure also suggests that the probability of a Stage 2 false negative error is very close to 0 for all but three species. One of these three (sp. 14) is in the fly family Tachinidae, which are parasitoids of other insects and thus might have been collected not only as adults but also occasionally as eggs attached to the adults of other (insect) host species, with the latter case being classified as false positives in Stage 2, given that an egg would contribute very low amounts of starting DNA biomass.

elfig:cov˙results

6 Discussion

Over the last decade, DNA-based biodiversity studies, primarily using metabarcoding, have rapidly increased in popularity, and multivariate statistical models are now starting to be deployed to analyse metabarcoding data (e.g. Lin et al., 2021; Pichler and Hartig, 2021; Abrego et al., 2021; Fukaya et al., 2022; Ji et al., 2022). Our paper provides the first unifying modelling framework that considers and quantifies key sources of variation, error and noise in metabarcoding surveys (Table 1). As a result, our modelling framework allows more reliable and more powerful biodiversity monitoring and inference on species

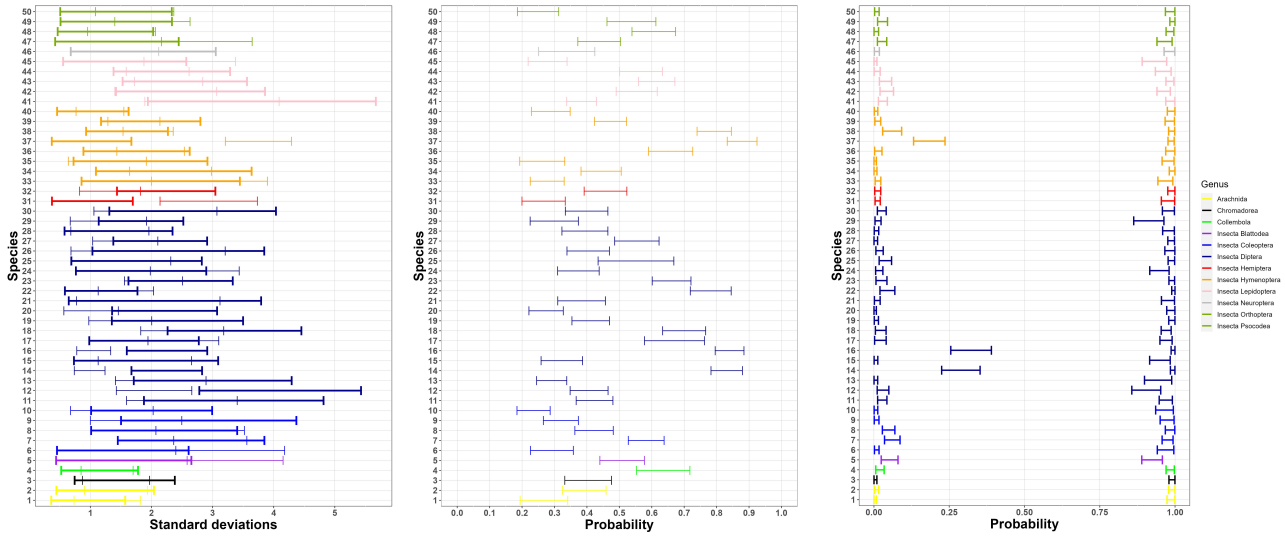

Figure 8: Case study: (left) 95% PCI of the species-specific between-samples standard deviation σ_s and between-sites standard deviation $\sqrt{T_{ss}}$ (in bold). (center) 95% PCI of the species-specific average collection probability θ^s_{im} across all sites. (right) 95% PCI of the species-specific Stage 2 false-positive probabilities q_s (on the left of the plot) and true-positive probabilities p_s (on the right of the plot). Species are grouped taxonomically.

responses to landscape characteristics than has been possible before. We have employed, extended, and developed a number of inferential tools to deal with the complexity of the proposed hierarchical model, which involves two latent stages and a large number of latent variables. Finally, this is the first modelling approach that accounts for spike-ins and negative controls (empty tubes), which are widely used quality-control methods in DNA-based biodiversity surveys but rarely explicitly considered within a modelling framework. We explored the benefits of spike-ins on inference and provided analytical and simulation results of the effects of study design choices on parameter estimates. As is the case in all models, we make certain assumptions about the data-generating process and if (any of) these assumptions are violated, then inference can be biased. Below, we discuss the key assumptions and corresponding model extensions, when appropriate.

Our new framework allows us to infer and map species DNA biomass change across surveyed sites (Figure 7 (b)), and to link these to landscape characteristics (Figure 6). The resulting maps can be used to identify areas of high conservation value, as well as areas where particular species or groups of species are more or less prevalent, and to detect species-specific shifts, expansions, and shrinkage. We are also able to study pairwise

correlations across large numbers of species (Figure 7 (a)), which is considerably more scalable using metabarcoding data than using standard observational data. We note that, as discussed in the corresponding sections of the model and the case study, we cannot unambiguously identify the sources of the estimated correlations using the available data alone, as factors other than the affinity between species, such as competition for primers, could affect the inferred species correlations. We have shown that using spike-ins can substantially increase inference accuracy for parameters of interest (Figure 5). Our results also demonstrate that the current practice of collecting a single sample from each surveyed site considerably reduces our ability to infer changes in species DNA biomass and that replication at both stages as well as the use of normalisation-ratio offsets or spike-ins is the optimal approach to designing metabarcoding studies (Figure 3).

In metabarcoding data, the baseline DNA biomass of each species is confounded with its species-specific collection and amplification rates. Hence, we cannot infer absolute values of species-specific DNA biomass across sites using metabarcoding data alone. However, by assuming that baseline species-specific collection and amplification rates are the same across sites, samples, and PCR replicates, we can infer species-specific DNA biomass *change* across sites, species-specific covariate effects, and pairwise species correlations. Finally, we model species amplification rates as independent random effects, but competition between species for primers, polymerases and nucleotides during PCR amplification might violate this independence assumption, and future experimental work, alongside model extensions, should explore this issue further.

We note that we have not allowed the probability of Stage 2 species detection, p_s, to vary between samples or PCR replicates, and hence we have assumed that it does not depend on the DNA biomass of other species in the sample/PCR replicate. However, because of the PCR product normalisation step, described in Section 1.1, in PCR replicates with relatively high resulting overall DNA biomass, relatively low-DNA-biomass species might be less likely to be drawn in high enough concentration to be detected, an issue that is

often referred to as PCR dropout. Empirically, it is known that such PCR competition can be mitigated by using a lower number of PCR cycles (Yang et al., 2021) and by sequencing each sample replicate more deeply. When extending the model of this paper, Stage 2 species detection can be modelled as a function of DNA biomass, so that $\text{logit}(p^s_{imk}) = \beta^p_0 + \beta_p(v^s_{im} + o_{imk})$. Model extensions of this type are important but are expected to introduce further identifiability issues and computational challenges and hence require careful investigation.

Generally, modelling changes in (proxies of) abundance, such as changes in DNA biomass, is a more powerful monitoring tool than modelling changes in species presence across survey sites (Joseph et al., 2006). Metabarcoding studies yield count data without any consequence on associated cost, and hence overcome the time and cost implications associated with collecting count data for multiple species. Our model uses the raw count data, and does not rely on ad-hoc rules about what constitutes a practically zero count for converting them to binary data, which has been the standard practice thus far (Ovaskainen et al., 2017; Bush et al., 2020). To model changes in (log)biomass for each species across sites, we rely on the investigator being able to record any normalisation steps (or to include a spike-in), otherwise the relationship between change in read counts and change in the amount of biomass in the environment cannot be inferred, and instead the counts can only be used to infer composition, as is standard practice in metabarcoding studies. We have allowed for over-dispersion in the count data using a negative binomial distribution, but future work could consider alternative parametrisations, such as the discrete Weibull distribution. The model can also be extended to account for multiple primers or for differences between labs, if samples are processed by more than one lab, by introducing regression models for corresponding parameters.

Metabarcoding studies, particularly when applied to microbiomes and meiofauna (e.g. nematodes, micro-eukaryotes), can detect 1000s of species, which leads to large numbers of latent variables and coefficients in the model. There are several ways that the inferential tools presented here could be further extended to scale to these cases. Firstly, the posterior

distribution conditional on the u_{imk} is independent across species. If u_{imk} could be estimated at a first stage then inference across species could be easily parallelized. Secondly, variational Bayes methods could be applied to avoid the use of sampling methods. The choice of variational distribution will be important and can exploit the conditional normality of much of the model. Alternatively, the model could be adapted by assuming that the coefficient matrices such as $\beta^z = (\beta_1^z, \ldots, \beta_S^z)$, have a low-dimensional representation. We highlight that in its current format, the model assumes species-specific parameters, and hence there is potentially a large number of parameters to be estimated for each species. Therefore, if a species only has a few non-zero PCR reads from potentially only a few sites, estimating all of these species-specific parameters is difficult. Future work should explore sharing parameters between species, making inference for rarely-observed species possible.

We are not modelling species presence/absence and instead we have focused on modelling biomass on a continuous scale. As a result, we cannot infer whether a species is absent from a particular study site, but instead only if its DNA biomass at a given site is practically zero. We have assumed that a sample which already contains DNA biomass of a species cannot be further contaminated by the DNA of the same species from another sample or site in Stage 1. This is a reasonable but also necessary assumption, because of model identifiability issues otherwise. It is possible that there exists contamination from other sites if their samples are all processed in the same laboratory, especially at the same time, or that there is contamination during the collection or transfer of samples. However, with only metabarcoding data to hand, it is not possible to identify the source of contamination, or to model the possibility that a sample that contains DNA of a species has been further contaminated by the DNA of the same species from another sample or site in Stage 1. This is yet another reason to take measures that minimise contamination risk.

eDNA metabarcoding has revolutionised the cost-effectiveness, precision, and scale at which biodiversity assessment can be performed. Nevertheless, the multiple stages at which imperfect detection of DNA biomass can occur during the workflow are not insignificant. By

facilitating estimates of within-species changes in DNA biomass as a function of covariates, while accounting for workflow uncertainties, our modelling framework provides a substantial improvement in the design and analysis of eDNA metabarcoding data.

Data Availability

The sequence data, bioinformatic scripts, and the three sample by species tables and environmental covariates are archived on DataDryad at doi.org/10.5061/dryad.4f4qrfjjb.

Acknowledgments

The work was funded by NERC project NE/T010045/1 "Integrating new statistical frameworks into eDNA survey and analysis at the landscape scale" and benefited from the sCom Working Group at iDiv.de. DWY and MJL were supported by the Strategic Priority Research Program of Chinese Academy of Sciences, Grant No. XDA20050202, the Key Research Program of Frontier Sciences, CAS (QYZDY-SSW-SMC024), the State Key Laboratory of Genetic Resources and Evolution (GREKF19-01, GREKF20-01, GREKF21-01) at the Kunming Institute of Zoology, and the University of Chinese Academy of Sciences.

Disclosure statement

The authors declare that there are no conflicts of interest relevant to this article.

References

Abrego, N., Roslin, T., Huotari, T., et al. (2021). Accounting for species interactions is necessary for predicting how arctic arthropod communities respond to climate change. *Ecography*, 44(6):885–896.

Andrieu, C. and Thoms, J. (2008). A tutorial on adaptive MCMC. *Statistics and Computing*, 18(4):343–373.

Baisero, D., Schuster, R., and Plumptre, A. J. (2022). Redefining and mapping global irreplaceability. *Conservation Biology*, 36(2):e13806.

Besson, M., Alison, J., Bjerge, K., et al. (2022). Towards the fully automated monitoring of ecological communities. *Ecological Letters*, to appear.

Bush, A., Monk, W. A., Compson, Z. G., et al. (2020). DNA metabarcoding reveals

metacommunity dynamics in a threatened boreal wetland wilderness. *Proceedings of the National Academy of Sciences*, 117(15):8539–8545.

Bush, A., Sollmann, R., Wilting, A., et al. (2017). Connecting Earth observation to high-throughput biodiversity data. *Nature Ecology & Evolution*, 1(7):0176.

Buxton, A., Matechou, E., Griffin, J., et al. (2021). Optimising sampling and analysis protocols in environmental DNA studies. *Scientific Reports*, 11(1):11637.

Carraro, L., Hartikainen, H., Jokela, J., et al. (2018). Estimating species distribution and abundance in river networks using environmental DNA. *Proceedings of the National Academy of Sciences*, 115(46):11724–11729.

Clare, E. L., Economou, C. K., Bennett, F. J., and others. (2022). Measuring biodiversity from DNA in the air. *Current Biology*, 32(3):693–700.e5.

Clausen, D. S. and Willis, A. D. (2022). Modeling complex measurement error in microbiome experiments. *arXiv preprint arXiv:2204.12733*.

Coblentz, K. E., Rosenblatt, A. E., and Novak, M. (2017). The application of Bayesian hierarchical models to quantify individual diet specialization. *Ecology*, 98(6):1535–1547.

Datta, J. and Dunson, D. B. (2016). Bayesian inference on quasi-sparse count data. *Biometrika*, 103:971—983.

Dawid, A. P. (1981). Some matrix-variate distribution theory: notational considerations and a Bayesian application. *Biometrika*, 68(1):265–274.

Ficetola, G. F., Pansu, J., Bonin, A., et al. (2015). Replication levels, false presences and the estimation of the presence/absence from eDNA metabarcoding data. *Molecular Ecology Resources*, 15(3):543–556.

Fordyce, J. A., Gompert, Z., Forister, M. L., and Nice, C. C. (2011). A hierarchical Bayesian approach to ecological count data: a flexible tool for ecologists. *PloS One*, 6(11):e26785.

Frøslev, T. G., Kjøller, R., Bruun, H. H., et al. (2019). Man against machine: Do fungal fruitbodies and eDNA give similar biodiversity assessments across broad environmental gradients? *Biological Conservation*, 233:201–212.

Fukaya, K., Kondo, N. I., Matsuzaki, S.-i. S., and Kadoya, T. (2022). Multispecies site occupancy modelling and study design for spatially replicated environmental DNA metabarcoding. *Methods in Ecology and Evolution*, 13(1):183–193.

Gelman, A. (2006). Prior distributions for variance parameters in hierarchical models. *Bayesian Analysis*, 1(3):515–533.

Griffin, J. E., Matechou, E., Buxton, A. S., et al. (2020). Modelling environmental DNA

763 data; Bayesian variable selection accounting for false positive and false negative errors.
764 *Journal of the Royal Statistical Society: Series C (Applied Statistics)*, 69(2):377–392.
765 Guillera-Arroita, G., Lahoz-Monfort, J., van Rooyen, A., Weeks, A., and Tingley, R. (2017).
766 Dealing with false-positive and false-negative errors about species occurrence at multiple
767 levels. *Methods in Ecology and Evolution*, 8(9):1081–1091.
768 Hebert, P. D., Cywinska, A., Ball, S. L., and DeWaard, J. R. (2003). Biological identifi-
769 cations through DNA barcodes. *Proceedings of the Royal Society of London. Series B:*
770 *Biological Sciences*, 270(1512):313–321.
771 Ji, Y., Ashton, L., Pedley, S. M., et al. (2013). Reliable, verifiable and efficient monitoring
772 of biodiversity via metabarcoding. *Ecology Letters*, 16(10):1245–1257.
773 Ji, Y., Baker, C. C. M., Popescu, V. D., et al. (2022). Measuring protected-area effectiveness
774 using vertebrate distributions from leech iDNA. *Nature Communications*, 13(1):1555.
775 Joseph, L. N., Field, S. A., Wilcox, C., and Possingham, H. P. (2006). Presence–absence ver-
776 sus abundance data for monitoring threatened species. *Conservation Biology*, 20(6):1679–
777 1687.
778 Ley, R. (2022). The human microbiome: there is much left to do. *Nature*,
779 606(7914):435–435.
780 Li, Y., Craig, B. A., and Bhadra, A. (2019). The graphical horseshoe estimator for inverse
781 covariance matrices. *Journal of Computational and Graphical Statistics*, 28(3):747–757.
782 Li, Y., Devenish, C., Tosa, et al. (2024). Combining environmental dna and remote sensing
783 for efficient, fine-scale mapping of arthropod biodiversity. *Philosophical Transactions of*
784 *the Royal Society B: Biological Sciences*, 379(1904):20230123.
785 Lin, M., Simons, A. L., et al. (2021). Landscape analyses using edna metabarcoding and
786 earth observation predict community biodiversity in california. *Ecological Applications*,
787 31(6):e02379.
788 Lindahl, B. D., Nilsson, R. H., Tedersoo, L., et al. (2013). Fungal community analysis
789 by high-throughput sequencing of amplified markers–a user's guide. *New Phytologist*,
790 199(1):288–299.
791 Luo, M., Ji, Y., Warton, D., and Yu, D. W. (2022). Extracting abundance information
792 from DNA-based data. *Molecular Ecology Resources*, to appear.
793 McLaren, M. R., Willis, A. D., and Callahan, B. J. (2019). Consistent and correctable bias
794 in metagenomic sequencing experiments. *Elife*, 8:e46923.
795 Mordecai, R. S., Mattsson, B. J., Tzilkowski, C. J., and Cooper, R. J. (2011). Addressing

challenges when studying mobile or episodic species: hierarchical Bayes estimation of occupancy and use. *Journal of Applied Ecology*, 48(1):56–66.

Ovaskainen, O. and Abrego, N. (2020). *Joint Species Distribution Modelling: With Applications in R*. Cambridge University Press.

Ovaskainen, O., Tikhonov, G., Dunson, D., et al. (2017). How are species interactions structured in species-rich communities? A new method for analysing time-series data. *Proceedings of the Royal Society B: Biological Sciences*, 284(1855):20170768.

Papaspiliopoulos, O., Roberts, G. O., and Sköld, M. (2007). A general framework for the parametrization of hierarchical models. *Statistical Science*, 22(1):59–73.

Papaspiliopoulos, O., Roberts, G. O., and Zanella, G. (2020). Scalable inference for crossed random effects models. *Biometrika*, 107(1):25–40.

Pichler, M. and Hartig, F. (2021). A new joint species distribution model for faster and more accurate inference of species associations from big community data. *Methods in Ecology and Evolution*.

Piper, A. M., Batovska, J., Cogan, N. O. I., et al. (2019). Prospects and challenges of implementing DNA metabarcoding for high-throughput insect surveillance. *GigaScience*, 8(8):giz092.

Ratnasingham, S. and Hebert, P. D. (2007). Bold: The barcode of life data system (http://www. barcodinglife. org). *Molecular Ecology Notes*, 7(3):355–364.

Roberts, G. O. and Rosenthal, J. S. (2009). Examples of adaptive MCMC. *Journal of Computational and Graphical Statistics*, 18(2):349–367.

Saine, S., Ovaskainen, O., Somervuo, P., and Abrego, N. (2020). Data collected by fruit body-and DNA-based survey methods yield consistent species-to-species association networks in wood-inhabiting fungal communities. *Oikos*, 129(12):1833–1843.

Schmidt, B. R., Kery, M., Ursenbacher, S., et al. (2013). Site occupancy models in the analysis of environmental DNA presence/absence surveys: a case study of an emerging amphibian pathogen. *Methods in Ecology and Evolution*, 4(7):646–653.

Taberlet, P., Bonin, A., Zinger, L., and Coissac, E. (2018). *Environmental DNA: for biodiversity research and monitoring*. Oxford University Press, Oxford, United Kingdom.

Takahara, T., Minamoto, T., Yamanaka, H., et al. (2012). Estimation of fish biomass using environmental DNA. *PloS one*, 7(4):e35868.

Thomsen, P. F. and Sigsgaard, E. E. (2019). Environmental DNA metabarcoding of wild flowers reveals diverse communities of terrestrial arthropods. *Ecology and Evolution*,

9(4):1665–1679.

Thomsen, P. F. and Willerslev, E. (2015). Environmental DNA – An emerging tool in conservation for monitoring past and present biodiversity. *Biological Conservation*, 183:4–18.

Tkacz, A., Hortala, M., and Poole, P. S. (2018). Absolute quantitation of microbiota abundance in environmental samples. *Microbiome*, 6(1):110.

Ver Hoef, J. M. and Boveng, P. L. (2007). Quasi-Poisson vs. Negative Binomial Regression: How Should We Model Overdispersed Count Data? *Ecology*, 88:2766–2772.

Wang, H. (2012). Bayesian graphical lasso models and efficient posterior computation. *Bayesian Analysis*, 7(4):867–886.

Yang, C., Bohmann, K., Wang, X., and others. (2021). Biodiversity Soup II: A bulk-sample metabarcoding pipeline emphasizing error reduction. *Methods in Ecology and Evolution*, 12(7):1252–1264.

Zanella, G. and Roberts, G. (2021). Multilevel linear models, Gibbs samplers and multigrid decompositions (with discussion). *Bayesian Analysis*, 16(4):1309–1391.

Supplementary material of eDNAPlus: A unifying modelling framework for DNA-based biodiversity monitoring

Alex Diana[1], Eleni Matechou[1], Jim Griffin[2], Douglas W. Yu[3,4,5], Mingjie Luo[4], Marie Tosa[5], Alex Bush[6], Richard Griffiths[7]

[1] School of Mathematics, Statistics and Actuarial Science, University of Kent, UK,

[2] Department of Statistical Science, University College London, UK,

[3] School of Biological Sciences, University of East Anglia, UK,

[4] Kunming College of Life Sciences, University of Chinese Academy of Sciences, China,

[5] Center for Excellence in Animal Evolution and Genetics &

State Key Laboratory of Genetic Resources and Evolution &

Yunnan Key Laboratory of Biodiversity and Ecological Security of Gaoligong Mountain &

Kunming Institute of Zoology, Chinese Academy of Sciences, Kunming, China,

[6] Department of Fisheries, Wildlife, & Conservation Sciences, Oregon State University, Oregon USA,

[7] Lancaster Environment Centre, University of Lancaster, UK,

[8] Durrell Institute of Conservation and Ecology, University of Kent, UK

September 29, 2024

1 Inference

We can reparameterise the model by expressing the negative binomial using the Poisson-Gamma mixture and a centred parameterisation:

$$
\begin{cases}
\bar{\beta}_0^s \sim \mathrm{N}(\lambda_s, \sigma_\beta^2) \\
\bar{L} = \{\bar{l}_i^s\} \sim \mathrm{MN}(\bar{B}_0 + X_z B, \Sigma, T) \\
T^{-1} \sim \mathrm{GH} \\
\mathrm{logit}(\theta_{im}^s) = (\bar{l}_i^s - \lambda_s)\phi_{1s} + X_{im}^w \phi_s \\
\mathbb{P}(\delta_{im}^s = 1) = \theta_{im}^s \\
\mathbb{P}(\gamma_{im}^s = 1 \mid \delta_{im}^s = 0) = \zeta^s \\
\bar{\mu}_s \sim \mathrm{N}(\lambda_s, \sigma_\mu^2) \\
\bar{v}_{im}^s \sim \begin{cases} \mathrm{N}(\bar{l}_i^s + X_{im}^w \beta_s^W, \sigma_s^2) & \text{if } \delta_{im}^s = 1 \\ \mathrm{N}(\bar{\mu}_s, \nu_s^2) & \text{if } \delta_{im}^s = 0, \gamma_{im}^s = 1 \end{cases} \\
\mathbb{P}(c_{imk}^s = 1 | \delta_{im}^s = 1 \text{ or } \gamma_{im}^s = 1) = p_s \\
\mathbb{P}(c_{imk}^s = 2 | \delta_{im}^s = 0, \gamma_{im}^s = 0) = q_s \\
\eta_{imk}^s \sim \mathrm{Gamma}\left(r_s, \frac{r_s}{\exp(\bar{v}_{im}^s + u_{imk} + o_{imk})}\right) \qquad \text{if } c_{imk}^s = 1 \\
y_{imk}^s \sim \begin{cases} \pi\delta_0 + (1-\pi)(1 + \mathrm{NB}(\mu_0, n_0)) & \text{if } c_{imk}^s = 0 \\ \mathrm{Pois}(\eta_{imk}^s) & \text{if } c_{imk}^s = 1 \\ \mathrm{Pois}(\tilde{\mu}) & \text{if } c_{imk}^s = 2 \end{cases} \\
u_{imk} \sim \mathrm{N}(0, \sigma_u^2)
\end{cases}
$$

where we have defined

$$
\begin{cases}
\bar{\beta}_0^s = \beta_0^s + \lambda_s \\
\bar{l}_i^s = l_i^s + \lambda_s \\
\bar{v}_{im}^s = v_{im}^s + \lambda_s \\
\bar{\mu}_s = \mu_s + \lambda_s
\end{cases}.
$$

If not stated, we use a Metropolis-Hastings update with a Laplace approximation as

proposal if a full conditional distribution is not tractable.

- Update λ_s

  The full conditional has the density

$$\mathrm{N}(\bar{\beta}_0^s|\lambda_s, \sigma_\beta^2)\ \mathrm{N}(\bar{\mu}_s|\lambda_s, \sigma_\mu^2) \left(\prod_{i,m} \mathrm{Be}\left(\delta_{im}^s, \mathrm{logit}(-\phi_{1s}\lambda_s + \phi_{1s}\bar{l}_i^s + X_{im}^w \phi_s)\right) \right)$$

  and the parameter is updated using a Metropolis-Hastings random walk.

- Update η_{imk}^s

$$\eta_{imk}^s \sim \mathrm{Gamma}\left(r_s + y_{imk}^s, 1 + \frac{r_s}{\exp(\bar{v}_{im}^s + u_{imk} + o_{imk})}\right)$$

- Update r_s

  The full conditional distribution has density

$$p(r_s|\cdot) \propto \mathrm{N}(r_s|\mu_r, \sigma_r^2) \prod_{i,m,k:c_{imk}^s=1} \mathrm{NB}(y_{imk}^s|\exp(\bar{v}_{im}^s + u_{imk} + o_{imk}), r_s)$$

  and the parameter is updated using a Metropolis-Hastings random walk.

- Update $\bar{v}_{im}^s$ and u_{imk}

  We define the overall means $\hat{v}_{im} = \frac{1}{n_{im}} \sum_{s:\delta_{im}^s=1 \text{ or } \gamma_{im}^s=1} \bar{v}_{im}^s$, where $n_{im} = \sum_{s:\delta_{im}^s=1 \text{ or } \gamma_{im}^s=1}$, and $\hat{u}_{im} = \frac{1}{K} \sum_k u_{imk}$, and the increments $\tilde{v}_{im}^s = \bar{v}_{im}^s - \hat{v}_{im}$ and $\tilde{u}_{imk} = u_{imk} - \hat{u}_{im}$.

  We first sample from the joint full conditional of the overall means conditional on the increments $(\hat{v}_{im}, \hat{u}_{im}|\tilde{v}_{im}^1, \ldots, \tilde{v}_{im}^S, \tilde{u}_{im1}, \ldots, \tilde{u}_{imK}, \ldots)$, which has density of the form

$$p(\hat{v}_{im}, \hat{u}_{im}|\cdot) \propto \mathrm{N}\left(\hat{v}_{im} \middle| \frac{1}{n_{im}} \sum_{s:\delta_{im}^s=1 \text{ or } \gamma_{im}^s=1} l_i^s, \frac{1}{n_{im}} \sum_{s:\delta_{im}^s=1 \text{ or } \gamma_{im}^s=1} \sigma_s^2\right) \mathrm{N}\left(\hat{u}_{im} \middle| 0, \frac{\sigma_u^2}{K_{im}}\right)$$

$$\prod_{k,s:\ c_{imk}^s=1} \mathrm{Gamma}\left(\eta_{imk}^s|r_s, \frac{r_s}{\exp(\hat{v}_{im} + \tilde{v}_{im}^s + \hat{u}_{im} + \tilde{u}_{imk} + o_{imk})}\right)$$

  where $n_{im} = \sum_{s:\delta_{im}^s=1}$.

Next, we sample $\bar{v}_{im}^s$ from its full conditional distribution which has density

$$p(\bar{v}_{im}^s|\cdot) \propto \mathrm{N}(\bar{v}_{im}^s|\bar{l}_i^s + X_{im}^w\beta_s^W, \sigma_s^2)^{\delta_{im}^s}\mathrm{N}(\bar{v}_{im}^s|\bar{\mu}_s, \nu_s^2)^{(1-\delta_{im}^s)\gamma_{im}^s} \times \prod_{k:\ c_{imk}^s=1} \mathrm{Gamma}\left(\eta_{imk}^s|r_s, \frac{r_s}{\exp(\bar{v}_{im}^s + u_{imk} + o_{imk})}\right),$$

and u_{imk} from its full conditional distribution which has density

$$p(u_{imk}|\cdot) \propto \mathrm{N}(u_{imk}|0, \sigma_u^2) \prod_{s:\ c_{imk}^s=1} \mathrm{Gamma}\left(\eta_{imk}^s|r_s, \frac{r_s}{\exp(\bar{v}_{im}^s + u_{imk} + o_{imk})}\right),$$

In all three cases, we use a Metropolis-Hastings update with a Laplace approximation as proposal.

- Update $\bar{l}_i^s$

  The parameter can be updated from its full conditional distribution which has density

$$p(\bar{l}_i^s|\cdot) \propto \mathrm{N}(\bar{l}_i^s|\bar{\beta}_0^s + X_i\beta_s^z, \bar{l}_{-i}^{-s}, T, \Sigma) \prod_{m:\delta_{im}^s=1} \mathrm{N}(\bar{v}_{im}^s|\bar{l}_i^s + X_{im}\beta_s^W, \sigma_s^2) \prod_m \mathrm{Be}(\delta_{im}^s|\mathrm{logit}\left(-\phi_{1s}\lambda + \phi_{1s}\bar{l}_i^s + X_{im}^W\phi_s\right))$$

  using a Metropolis-Hastings update with a Laplace approximation as proposal. The conditional distribution $\mathrm{N}(\bar{l}_i^s|\bar{\beta}_0^s + X_i\beta_s^z, \bar{l}_{-i}^{-s}, T, \Sigma)$ can be efficiently computed using the algorithm described in Section 1.1.

- Update (B_0, B)

  These parameters are updated from their joint full conditional distribution which is

$$p(B_0, B|l) \propto \mathrm{N}(\mathrm{vec}((B_0, B))|0, \sigma_\beta^2 I_{(p+1)S})\mathrm{MN}(B_0 + X_z B, \Sigma, T)$$

  and can be written in closed form as

$$\mathrm{vec}(B_0, B) \sim \mathrm{N}(\Lambda_B^{-1}\mu_B, \Lambda_B^{-1})$$

where $\Lambda_B = T^{-1} \otimes (\bar{X}^T \Sigma^{-1} \bar{X})$ and $\mu_B = (I_S \otimes \bar{X}^T)(\Sigma^{-1} \text{vec}(L) T^{-1})$, with $\bar{X} = (1, X)$

- Update β_s^w

$$\beta_s^w \sim \text{N}(\Lambda_\beta^{-1} \mu_\beta, \Lambda_\beta^{-1})$$

where $\Lambda_\beta^{-1} = \frac{(X_\delta^W)^T X^W}{\sigma_s^2} + \sigma_\beta^2 I_{n_w}$ and $\mu_\beta = \frac{(X_v^W)^T}{\sigma_s^2}(v_\delta^s - l_\delta^s)$, and X_δ^W, v_δ^s, l_δ^s are the subset of X^w, v^s and l^s, respectively, such that $\delta_{im}^s = 1$ for species s.

- Update σ_s^2

$$\sigma_s^2 \sim \text{IG}(a_\sigma + n_\delta, b_\sigma + s_\delta)$$

where $n_\delta = \sum_{i,m} 1_{\delta_{i,m}^s = 1}$ and $s_\delta = \sum_{i,m:\delta_{i,m}^s=1} (\bar{v}_{im}^s - \bar{l}_i^s - X_{im}^w \beta_s^w)^2$.

- Update $\bar{\mu}_s$

$$\bar{\mu}_s \sim \text{N}(m_\mu, \sigma_\mu^2)$$

where $\sigma_\mu^2 = (\frac{1}{\sigma_\mu^2} + \frac{n_\gamma}{\nu_s^2})^{-1}$, $m_\mu = \left(\frac{\lambda_s}{\sigma_\mu^2} + \frac{\sum_{\gamma_{im}^s=1} \bar{v}_{im}^s}{\nu_s^2} \right) \sigma_\mu^2$ and $n_\gamma = \sum_{i,m} 1_{\gamma_{im}^s = 1}$

- Update ϕ_{1s} and ϕ_s.

Since these are coefficients of a logistic regression, we use the Pólya-gamma updating scheme (Polson et al., 2013) where δ_{im}^s are responses and the regressors are $\bar{l}_i^s - \lambda_s$ and X_{im}^w.

- Update c_{imk}^s, δ_{im}^s and γ_{im}^s

We update $c_{im1}^s, \ldots, c_{imK}^s$, δ_{im}^s and γ_{im}^s in a single block and, for ease of notation, we drop the indices i, m and s when describing the update. During the burn-in phase, we update these parameters by sampling from their full conditional distribution. We note that since the variable $\bar{v}$ is not present in the model if $\delta = \gamma = 0$, this update requires a reversible jump Markov Chain Monte Carlo (RJMCMC) move.

If $\delta \neq 0$ or $\gamma \neq 0$, we propose $c_1, \ldots, c_K$, δ and γ from their joint distribution evaluated using the currently sampled value of $v^\star$. Otherwise, we propose $v^\star$ using the informed

proposal $v^\star \sim \mathrm{N}(\mu^\star, .5^2)$, where $\exp(\mu^\star) = \frac{1}{K}\sum_{k=1}^{K} \frac{y^s_{imk}}{\exp(\lambda_s + u_{imk})}$ and propose $c_1, \ldots, c_K$, δ and γ from their joint distribution evaluated using this proposed value.

Using the notation $\delta^\star$, $\gamma^\star$ and $c^\star$ for the proposed value, the Metropolis-Hastings acceptance ratio are as follows. If $\delta = \gamma = 0$, the MH ratio takes the form

$$\begin{array}{ll} \min\left\{1, \frac{p(y_1,\ldots,y_K|\delta^\star=0,\gamma^\star=0,c_1^\star,\ldots,c_K^\star)p(\delta^\star=0,\gamma^\star=0,c_1^\star,\ldots,c_K^\star)q(\delta=0,\gamma=0,c_1,\ldots,c_K)}{p(y_1,\ldots,y_K|\delta=0,\gamma=0,c_1,\ldots,c_K)p(\delta=0,\gamma=0,c_1,\ldots,c_K)q(\delta^\star=0,\gamma^\star=0,c_1^\star,\ldots,c_K^\star)}\right\} & \text{if } \delta^\star = \gamma^\star = 0 \\ \min\left\{1, \frac{p(y_1,\ldots,y_K|\delta^\star=1,\gamma^\star=1,c_1^\star,\ldots,c_K^\star,v^\star)p(\delta^\star=1,\gamma^\star=1,c_1^\star,\ldots,c_K^\star)q(\delta=0,\gamma=0,c_1,\ldots,c_K)p(v^\star)}{p(y_1,\ldots,y_K|\delta=0,\gamma=0,c_1,\ldots,c_K)p(\delta=0,\gamma=0,c_1,\ldots,c_K)q(\delta^\star=1,\gamma^\star=1,c_1^\star,\ldots,c_K^\star,v^\star)}\right\} & \text{if } \delta^\star + \gamma^\star = 1 \end{array}$$

or, if $\delta + \gamma = 1$

$$\begin{array}{ll} \min\left\{1, \frac{p(y_1,\ldots,y_K|\delta^\star=1,\gamma^\star=1,c_1^\star,\ldots,c_K^\star,v)p(\delta^\star=1,\gamma^\star=1,c_1^\star,\ldots,c_K^\star)p(v)q(\delta=1,\gamma=1,c_1,\ldots,c_K,v)}{p(y_1,\ldots,y_K|\delta=1,\gamma=1,c_1,\ldots,c_K,v)p(\delta=1,\gamma=1,c_1,\ldots,c_K)p(v)q(\delta^\star=1,\gamma^\star=1,c_1^\star,\ldots,c_K^\star,v)}\right\} & \text{if } \delta^\star + \gamma^\star = 1 \\ \min\left\{1, \frac{p(y_1,\ldots,y_K|\delta^\star=0,\gamma^\star=0,c_1^\star,\ldots,c_K^\star)p(\delta^\star=0,\gamma^\star=0,c_1^\star,\ldots,c_K^\star)q(\delta=1,\gamma=1,c_1,\ldots,c_K,v)}{p(y_1,\ldots,y_K|\delta=1,\gamma=1,c_1,\ldots,c_K,v)p(v^\star)p(\delta=1,\gamma=1,c_1,\ldots,c_K)q(\delta^\star=0,\gamma^\star=0,c_1^\star,\ldots,c_K^\star)}\right\} & \text{if } \delta^\star = \gamma^\star = 0 \end{array}$$

Given a proposal $q(v)$, the algorithm can be made into a Gibbs sampler by choosing the proposals

$$q(\delta = 1, \gamma = 1, c_1, \ldots, c_K|v) \propto \frac{p(y_1, \ldots, y_K|\delta = 1, \gamma = 1, v)p(v)p(\delta = 1, \gamma = 1, c_1, \ldots, c_K)}{q(v)}$$

$$q(\delta = 0, \gamma = 0, c_1, \ldots, c_K|v) \propto p(y_1, \ldots, y_K|\delta = 0, \gamma = 0, v)p(\delta = 0, \gamma = 0, c_1, \ldots, c_K).$$

After the burn-in phase, we do not perform a full Gibbs sampler by computing the probability of every state but propose a new state $(\delta^\star, \gamma^\star, c_1^\star, \ldots, c_K^\star)$ from the approximation $\hat{p}(\delta^s_{im}, \gamma^s_{im}, c^s_{imk})$ described in the main text, which is accepted using the MH ratio defined above.

- Update T

  The precision matrix can be updated following the approach described by Li et al. (2019) and Wang (2012). Briefly, we introduce the variables ν_{ij} and ξ as in Makalic and Schmidt

(2015) as

$$\begin{cases} \omega_{ii} \propto \text{Exp}(\frac{\lambda}{2}) \\ \omega_{ij:i<j} \sim \text{N}(0, \lambda_{ij}^2 \tau^2) \\ \lambda_{ij:i<j}^2 \sim \text{IG}\left(\frac{1}{2}, \frac{1}{\nu_{ij}}\right) \\ \nu_{ij:i<j} \sim \text{IG}(\frac{1}{2}, 1) \\ \tau^2 \sim \text{IG}\left(\frac{1}{2}, \frac{1}{\xi}\right) \\ \xi \sim \text{IG}(\frac{1}{2}, 1) \end{cases}.$$

The rest of the parameters can be updated straightforwardly.

- Update p_s

$$p_s \sim \text{Beta}(a_p + n_{p_s}, b_p + m_{p_s} - n_{p_s})$$

where $n_{p_s} = \sum_{i,m,k} 1_{\delta_{im}^s + \gamma_{im}^s = 1, c_{imk}^s = 1}$ and $m_{p_s} = \sum_{i,m,k} 1_{\delta_{im}^s + \gamma_{im}^s = 1}$

- Update q_s

$$q_s \sim \text{Beta}(a_q + n_{q_s}, b_q + m_{q_s} - n_{q_s})$$

where $n_{q_s} = \sum_{i,m,k} 1_{\delta_{im}^s = 0, \gamma_{im}^s = 0, c_{imk}^s = 2}$ and $m_{q_s} = \sum_{i,m,k} 1_{\delta_{im}^s = 0, \gamma_{im}^s = 0}$

- Update $\tilde{\mu}$

This parameter is update using a MH with random walk proposal

- Update ζ_s

$\zeta_s \sim \text{Beta}(a_\zeta + n_\zeta, b_\zeta + m_\zeta - n_\zeta)$ where $n_\zeta = \sum_{i,m} 1_{\delta_{i,m}^s = 0, \gamma_{i,m}^s = 1}$ and $m_\zeta = \sum_{i,m} 1_{\delta_{i,m}^s = 0}$.

- Update π, μ_0, n_0

$$\pi \sim \text{Beta}(a_\pi + N_0, b_\pi + M_0 - N_0)$$

where $M_0 = \sum_{s,i,m,k} 1_{c_{imk}^s = 0}$ and $N_0 = \sum_{s,i,m,k} 1_{c_{imk}^s = 0, y_{imk}^s = 0}$.

μ_0 and n_0 are updated using a MH with random walk proposal.

1.1 Full conditional of matrix normal distributions

Proposition 1.1. *Given $x \sim MN(\mu, U, V)$, the full conditional distribution $x_{i,j}|x_{-(i,j)}$ has the form $N(\tilde{\mu}_{(i,j)}, \tilde{\sigma}^2_{(i,j)})$, where $\tilde{\mu}_{(i,j)}$ and $\tilde{\sigma}^2_{(i,j)}$ can be computed according to the following algorithm:*

1. *Compute x_1 by solving $U_{-i,-i}x_1 = U_{-i,i}$.*
2. *Compute $\tilde{\sigma_{i,j}}^2$ as $V_{j,j}U_{i,i} - (V_{j,j} \otimes U_{-i,i})x_1 + U_{i,i}\tilde{V} - (U_{i,-i} \cdot x_1)\tilde{V}$, where $\tilde{V} = (V_{j,-j} \cdot V^{-1}_{-j,-j} \cdot V_{-j,j})$*
3. *Compute y_1 by solving $U_{-i,-i}y_1 = \frac{\mu_{(-i,j)} - \mu_{(-i,-j)}\tilde{V}_2}{V_{j,j} - \tilde{V}}$, where $\tilde{V}_2 = (V_{1,-1} \cdot V^{-1}_{-1,-1})$.*
4. *Compute $\tilde{\mu}_{i,j}$ as $\mu_{(i,j)} + (V_{j,j} \otimes U_{-i,i})y_1 + \mu_{(i,-j)} \cdot \tilde{V}_2 - \tilde{V} \cdot U_{i,-i} \cdot y_1$.*

1.2 Proof

$\tilde{\mu}_{(i,j)}$ and $\tilde{\sigma}^2_{(i,j)}$ satisfy the equations

$$\tilde{\mu}_{(i,j)} = \mu_{(i,j)} + \Sigma_{(i,j),-(i,j)}\Sigma^{-1}_{-(i,j),-(i,j)}\mu_{-(i,j),(i,j)}$$

and

$$\tilde{\sigma}^2_{(i,j)} = \Sigma_{(i,j),(i,j)} - \Sigma_{(i,j),-(i,j)}\Sigma^{-1}_{-(i,j),-(i,j)}\Sigma_{-(i,j),(i,j)},$$

where $\Sigma = V \otimes U$.

W.l.o.g. we set $i = j = 1$. Let us define

$$\Sigma_{-(1,1),-(1,1)} = \begin{bmatrix} V_{11} \otimes U_{-1,-1} & V_{1,-1} \otimes U_{-1,\cdot} \\ V_{-1,1} \otimes U_{\cdot,-1} & V_{-1,-1} \otimes U \end{bmatrix} = \begin{bmatrix} \tilde{\Sigma}_{11} & \tilde{\Sigma}_{12} \\ \tilde{\Sigma}_{21} & \tilde{\Sigma}_{22} \end{bmatrix}$$

$$\Sigma_{-(1,1),(1,1)} = \begin{bmatrix} V_{11} \otimes U_{-1,1} \\ V_{-1,1} \otimes U_{\cdot,1} \end{bmatrix} = \begin{bmatrix} \tilde{b}_1 \\ \tilde{b}_2 \end{bmatrix} = \tilde{b}$$

$$\mu_{-(1,1),(1,1)} = \begin{bmatrix} \mu_{(-1,1)} \\ \mu_{(\cdot,-1)} \end{bmatrix} = \begin{bmatrix} \tilde{\mu}_1 \\ \tilde{\mu}_2 \end{bmatrix}$$

To compute $\tilde{\sigma}^2_{(1,1)}$, we need to compute $\Sigma_{(1,1),-(1,1)} \underbrace{\Sigma^{-1}_{-(1,1),-(1,1)}\Sigma_{-(1,1),(1,1)}}_{x}$. Computing x is equivalent to solving $\Sigma_{-(1,1),-(1,1)}x = \tilde{b}$. Using Schur complement, this is equivalent to solving $\underbrace{(\tilde{\Sigma}_{11} - \tilde{\Sigma}_{12}\tilde{\Sigma}^{-1}_{22}\tilde{\Sigma}_{21})}_{A} x_1 = \tilde{b_1} - \tilde{\Sigma}_{12}\tilde{\Sigma}^{-1}_{22}\tilde{b}_2$ and then $\tilde{\Sigma}_{22}x_2 = \tilde{b_2} - \tilde{\Sigma}_{21}x_1$.

Simplifications are available.

$$A = V_{1,1} \otimes U_{-1,-1} - \underbrace{(V_{1,-1} \cdot V^{-1}_{-1,-1} \cdot V_{-1,1})}_{\tilde{V}} \otimes (U_{-1,\cdot} \cdot U^{-1} \cdot U_{\cdot,-1}) =$$

$$V_{1,1} \otimes U_{-1,-1} - \tilde{V} \otimes (U_{-1,-1}) = (V_{1,1} - \tilde{V}) \cdot U_{-1,-1}$$

and

$$\tilde{b_1} - \tilde{\Sigma}_{12}\tilde{\Sigma}^{-1}_{22}\tilde{b}_2 = V_{11} \otimes U_{-1,1} - (V_{1,-1} \cdot V^{-1}_{-1,-1} \cdot V_{-1,1}) \otimes U_{-1,1} = (V_{1,1} - \tilde{V})U_{-1,1}$$

and therefore x_1 can be computed by solving $U_{-1,-1}x_1 = U_{-1,1}$.

Next,

$$x_2 = \tilde{\Sigma}^{-1}_{22}(\tilde{b_2} - \tilde{\Sigma}_{21}x_1) = (V^{-1}_{-1,-1} \otimes U^{-1})(V_{-1,1} \otimes U_{\cdot,1} - (V_{-1,1} \otimes U_{\cdot,-1})x_1) =$$

$$(V^{-1}_{-1,-1} \cdot V_{-1,1}) \otimes (U^{-1} \cdot U_{\cdot,1}) - (V^{-1}_{-1,-1} \cdot V_{-1,1}) \otimes (U^{-1} \cdot U_{\cdot,-1})x_1$$

and therefore $\tilde{b}_2x_2 = (V_{-1,1} \otimes U_{\cdot,1})x_2 = \tilde{V} \otimes (U_{\cdot,1} \cdot U^{-1} \cdot U_{\cdot,1}) - \tilde{V} \otimes (U_{\cdot,1} \cdot U^{-1} \cdot U_{\cdot,-1})x_1 = U_{1,1}\tilde{V} - (U_{1,-1} \cdot x_1)\tilde{V}$.

To compute $\tilde{\mu}_{(1,1)}$, we need to compute $\Sigma_{(1,1),-(1,1)} \underbrace{\Sigma^{-1}_{-(1,1),-(1,1)}\mu_{-(1,1),(1,1)}}_{y}$. Therefore, we have to solve $Ay_1 = \tilde{\mu_1} - \underbrace{(V_{1,-1} \cdot V^{-1}_{-1,-1})}_{\tilde{V}_2} \otimes (U_{-1,\cdot} \cdot U^{-1})\tilde{\mu}_2 = \tilde{\mu_1} - (\tilde{V}_2 \otimes e_1)\tilde{\mu}_2 = \tilde{\mu_1} - (\tilde{\mu}_2)_{1,\cdot}\tilde{V}_2$.

Since $A = (V_{1,1} - \tilde{V}) \cdot U_{-1,-1}$, we can find y_1 by solving $U_{-1,-1}y_1 = \frac{\tilde{\mu_1} - (\tilde{\mu}_2)_{1,\cdot}\tilde{V}_2}{V_{1,1} - \tilde{V}}$

Next, $y_2 = \tilde{\Sigma}^{-1}_{22}(\tilde{\mu_2} - \tilde{\Sigma}_{21}y_1) = (V^{-1}_{-1,-1} \otimes U^{-1})(\tilde{\mu_2} - (V_{-1,1} \otimes U_{\cdot,-1})y_1)$ and therefore

$$\tilde{\Sigma}_{12}\tilde{\Sigma}^{-1}_{22}(\tilde{\mu_2} - \tilde{\Sigma}_{21}y_1) = (V_{1,-1} \cdot V^{-1}_{-1,-1}) \otimes (U_{1,\cdot} \cdot U^{-1})(\tilde{\mu_2} - (V_{-1,1} \otimes U_{\cdot,-1})y_1) =$$

$$(\tilde{V}_2 \otimes e_1)\tilde{\mu}_2 - \tilde{V} \cdot U_{1,-1} \cdot y_1 = (\tilde{\mu}_2)_{1,\cdot}\tilde{V}_2 - \tilde{V} \cdot U_{1,-1} \cdot y_1$$

The last equation leads to the algorithm.

2 Prior settings

We use the following prior settings:

- $\sigma_\beta^2 = 1$
- We set Σ such that the (i, j) element $\Sigma_{i,j} = e^{\left(-\frac{1}{2l_\Sigma} d(s_i, s_j)^2\right)}$, where $d(s_i, s_j)$ is the distance between site i and site j and l_Σ is a scale parameter modeling the spatial autocorrelation. We have set the scale parameters $l_\Sigma = .05$.
- $a_\zeta = 1$, $b_\zeta = 50$
- $\sigma_\mu = 1$, $\nu_s = 1$
- $a_p = 20$, $b_p = 1$
- $a_q = 1$, $b_q = 100$
- $\mu_r = 100$, $\sigma_r = 100$

3 Simulation study settings

3.1 Study design simulations

For the differences in DNA biomasses, we set:

- $S = 40$
- $\tau = .5$, $\sigma = .5$, $\sigma_u = 1$
- $\beta_0 = 0$
- $\lambda_s \sim \mathrm{N}(7, 1)$
- $r_s = 100$
- $\phi_0 \sim \mathrm{N}(-1.5, .001)$

- $\zeta^s = .02$, $\nu_s = 1$
- $p = .95$, $q = .05$
- $\mu_0 = 5$, $n_0 = 5$, $\pi = .9$
- $\tilde{\mu} = 100$

We used the same settings for the covariate coefficients, but we also selected $\beta_s^z = \begin{cases} 1 & i \text{ odd} \\ 0 & i \text{ even.} \end{cases}$.

3.2 Spike-in simulations

For the differences in DNA biomasses, we set:

- $n = 100$
- $S = 10$
- $\sigma_u = 1$
- $\lambda_s \sim \mathrm{N}(7, 1)$
- $r_s = 100$

For the covariate coefficients, the settings were analogous but we set $n = 300$.

4 Additional plots on sampling

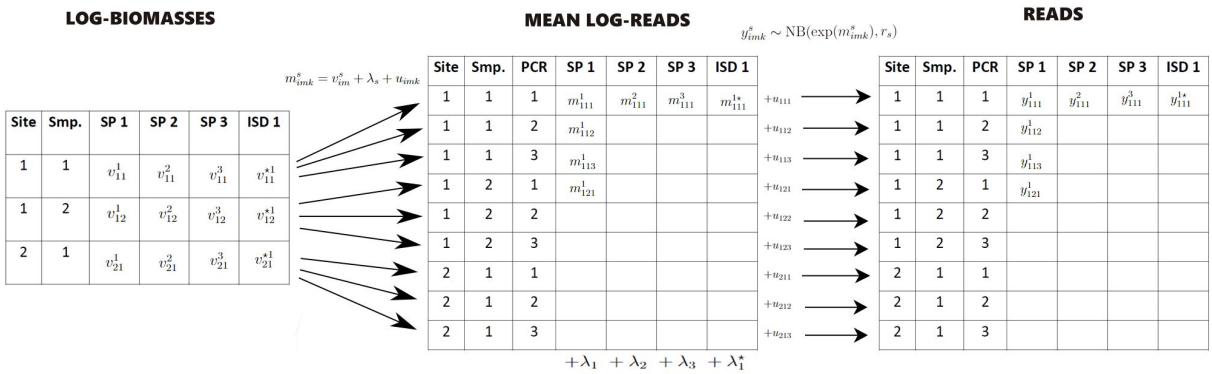

Figure 1: Representation of the biomass analysis stage. The number of reads (on the log scale) obtained for species s, in site i, sample m, and PCR k, is denoted by y^s_{imk} and is a function of the amount of log-biomass of that species in the corresponding sample (u^s_{im}), of the species effect, λ_s, which is common across samples and PCR runs, and of PCR noise, u_{imk}, which is common across species.

5 Additional plots on case study

1	Arachnida Araneae Anyphaenidae Anyphaena Anyphaena pacifica
2	Arachnida Opiliones Phalangiidae Leptobunus Leptobunus parvulus
3	Chromadorea Rhabditida Aphelenchoididae Bursaphelenchus Bursaphelenchus abruptus
4	Collembola Entomobryidae Family˙indet Genus˙indet Species˙indet
5	Insecta Blattodea Archotermopsidae Zootermopsis Zootermopsis angusticollis
6	Insecta Coleoptera Family˙indet Genus˙indet Species˙indet
7	Insecta Coleoptera Cerambycidae Leptura Leptura obliterata
8	Insecta Coleoptera Elateridae Hypoganus Species˙indet
9	Insecta Coleoptera Elateridae Megapenthes Megapenthes caprella
10	Insecta Coleoptera Scraptiidae Anaspis Anaspis rufa
11	Insecta Diptera Asilidae Genus˙indet Species˙indet
12	Insecta Diptera Tabanidae Hybomitra Species˙indet
13	Insecta Diptera Tabanidae Hybomitra Hybomitra liorhina
14	Insecta Diptera Tachinidae Eucelatoria Species˙indet
15	Insecta Diptera Scathophagidae Scathophaga Scathophaga furcata
16	Insecta Diptera Muscidae Phaonia Species˙indet
17	Insecta Diptera Family˙indet Genus˙indet Species˙indet
18	Insecta Diptera Syrphidae Hadromyia Hadromyia pulchra
19	Insecta Diptera Muscidae Spilogona Spilogona bifimbriata
20	Insecta Diptera Scathophagidae Microprosopa Species˙indet
21	Insecta Diptera Empididae Genus˙indet Species˙indet
22	Insecta Diptera Cecidomyiidae Genus˙indet Species˙indet
23	Insecta Diptera Anthomyiidae Genus˙indet Species˙indet
24	Insecta Diptera Mycetophilidae Cordyla Species˙indet
25	Insecta Diptera Phoridae Megaselia Species˙indet
26	Insecta Diptera Mycetophilidae Genus˙indet Species˙indet
27	Insecta Diptera Keroplatidae Genus˙indet Species˙indet
28	Insecta Diptera Sciaridae Genus˙indet Species˙indet
29	Insecta Diptera Rhagionidae Genus˙indet Species˙indet
30	Insecta Diptera Muscidae Helina Helina troene
31	Insecta Hemiptera Reduviidae Zelus Zelus tetracanthus
32	Insecta Hemiptera Cicadellidae Osbornellus Osbornellus borealis
33	Insecta Hymenoptera Formicidae Lasius Lasius pallitarsis
34	Insecta Hymenoptera Formicidae Camponotus Camponotus modoc
35	Insecta Hymenoptera Formicidae Leptothorax Species˙indet
36	Insecta Hymenoptera Vespidae Dolichovespula Dolichovespula maculata
37	Insecta Hymenoptera Vespidae Vespula Vespula alascensis
38	Insecta Hymenoptera Ichneumonidae Genus˙indet Species˙indet
39	Insecta Hymenoptera Vespidae Dolichovespula Dolichovespula alpicola
40	Insecta Hymenoptera Diapriidae Genus˙indet Species˙indet
41	Insecta Lepidoptera Geometridae Lambdina Lambdina fiscellaria
42	Insecta Lepidoptera Family˙indet Genus˙indet Species˙indet
43	Insecta Lepidoptera Geometridae Neoalcis Neoalcis californiaria
44	Insecta Lepidoptera Geometridae Ceratodalia Ceratodalia gueneata
45	Insecta Lepidoptera Geometridae Eulithis Eulithis destinata
46	Insecta Neuroptera Hemerobiidae Hemerobius Species˙indet
47	Insecta Orthoptera Rhaphidophoridae Pristoceuthophilus Pristoceuthophilus cercalis
48	Insecta Psocodea Caeciliusidae Valenzuela Species˙indet
49	Insecta Psocodea Dasydemellidae Teliapsocus Teliapsocus conterminus
50	Insecta Psocodea Psocidae Loensia Loensia maculosa

Table 1: Species used in the case study

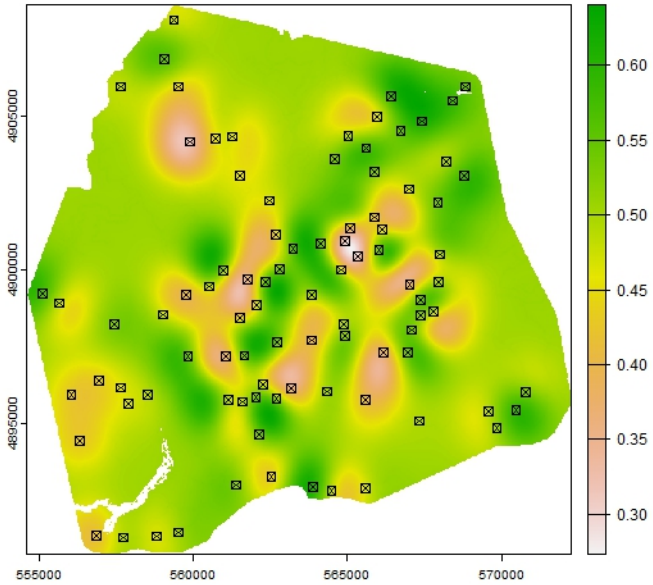

Figure 2: Biodiversity map with sampling points.

6 Comparison with existing methods

We compare our model with two existing approaches, a jSDM using the package *gllvm* and the two-stage occupancy model of Griffin et al. (2020).

6.1 gllvm

We use the *gllvm* package to fit a jSDM model based on a factor representation of the form

$$Y_i^s \sim \text{Pois}(\exp(X_i\beta_s + U_{i\cdot}\Lambda_{\cdot s}))$$

where Y_i^s are the counts of species s in sample i aggregated over the 3 PCRs, β_s are species-specific covariate coefficients and an estimate of the between-species covariance matrix is given by $\Lambda\Lambda^T$.

We use the same covariates as the case study: log-elevation and log-distance to road and summarise the estimated coefficients in In Fig. 8, while in Fig. 9 we report the residual covariance matrix of the observations.

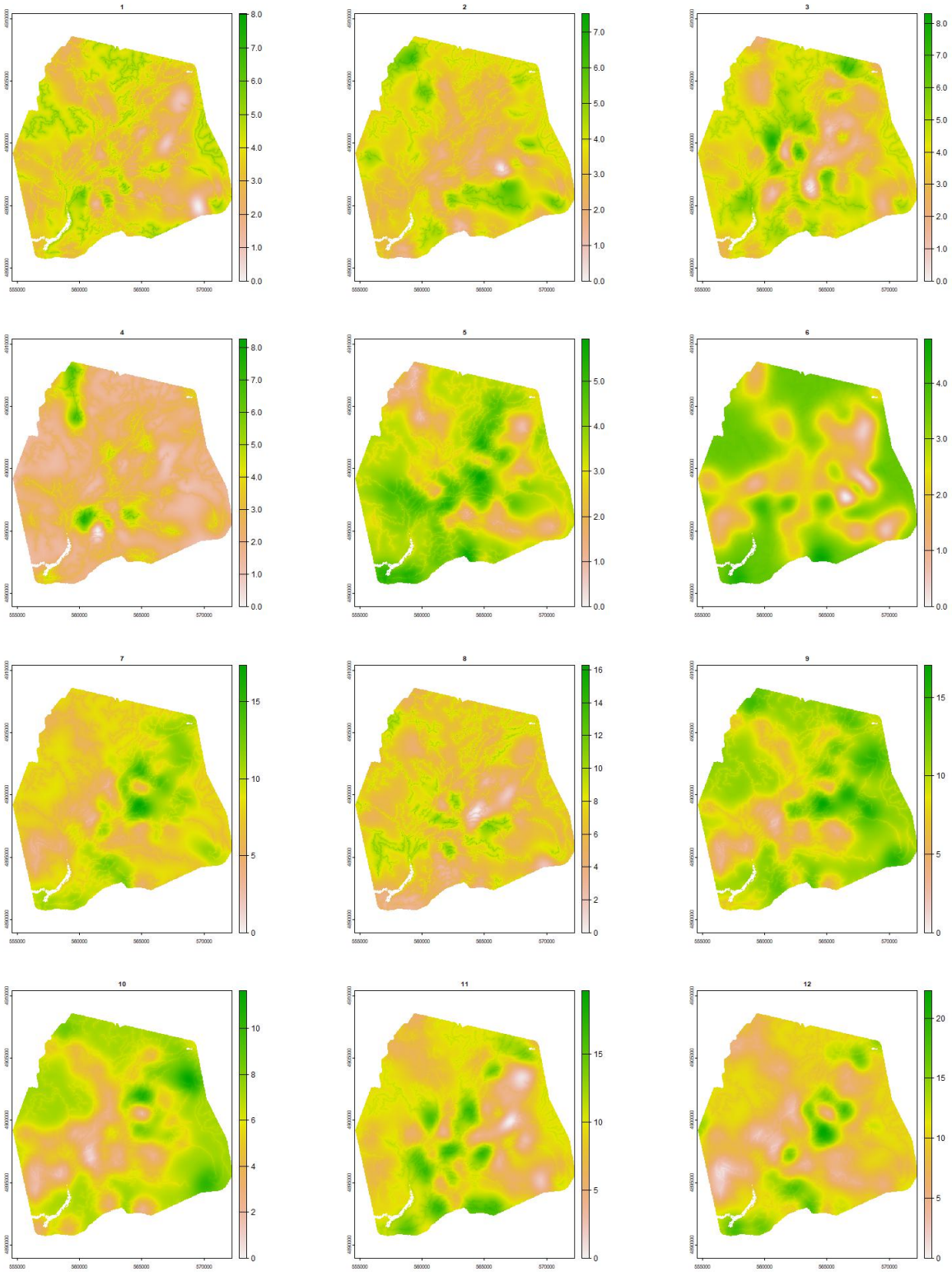

Figure 3: Maps of posterior mean log-biomass for species 1 to 12.

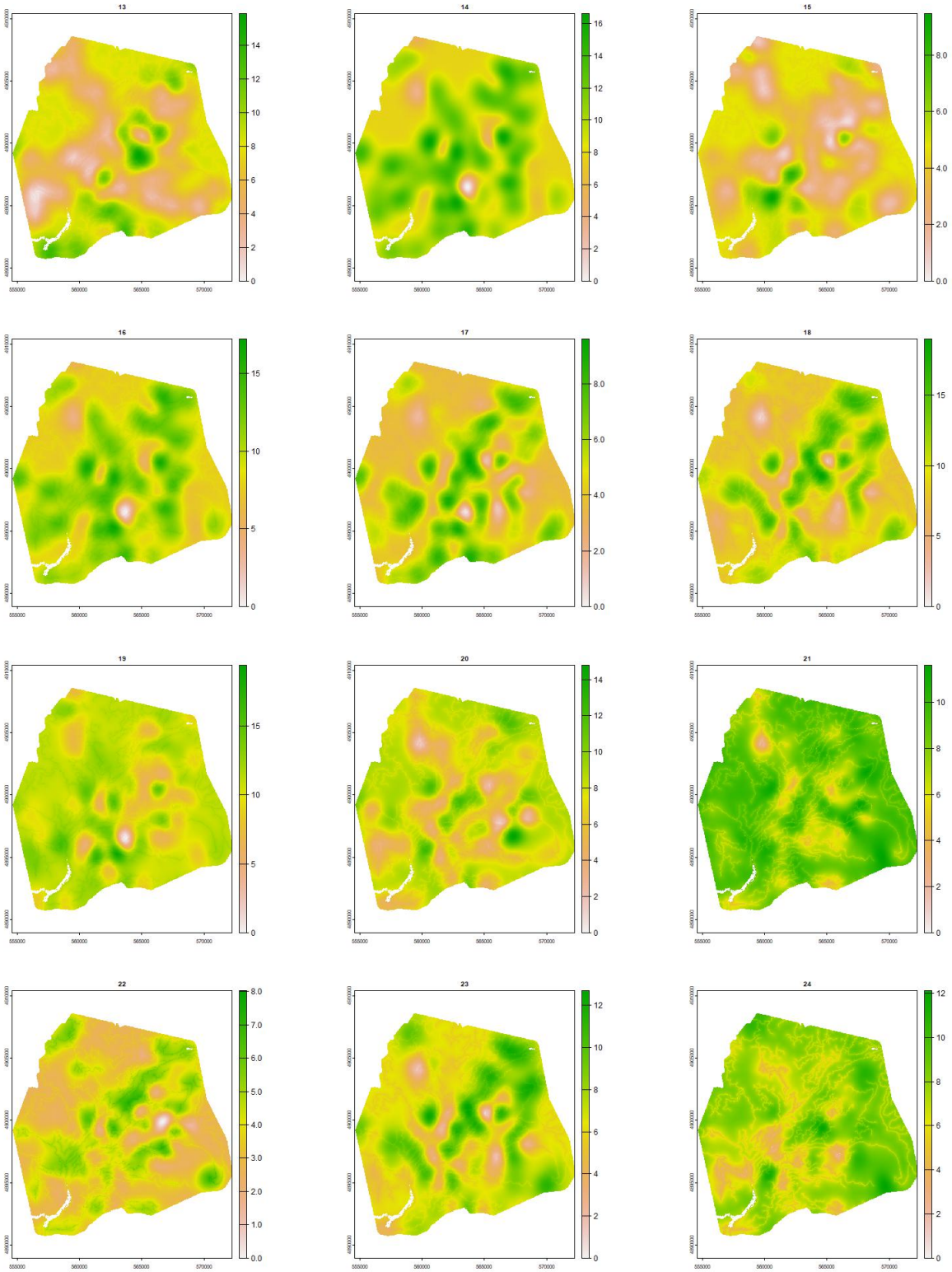

Figure 4: Maps of posterior mean log-biomass for species 13 to 24.

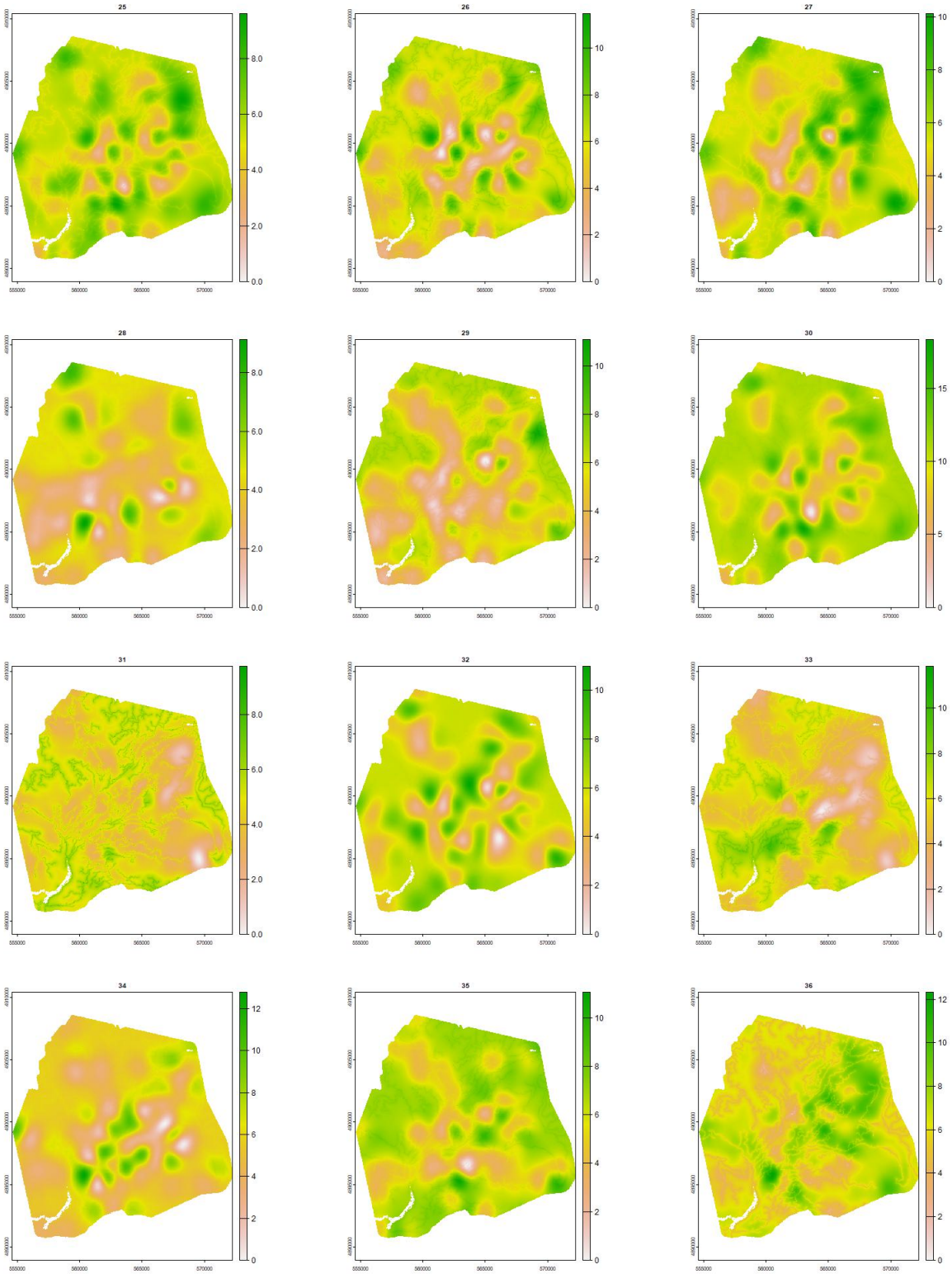

Figure 5: Maps of posterior mean log-biomass for species 25 to 36.

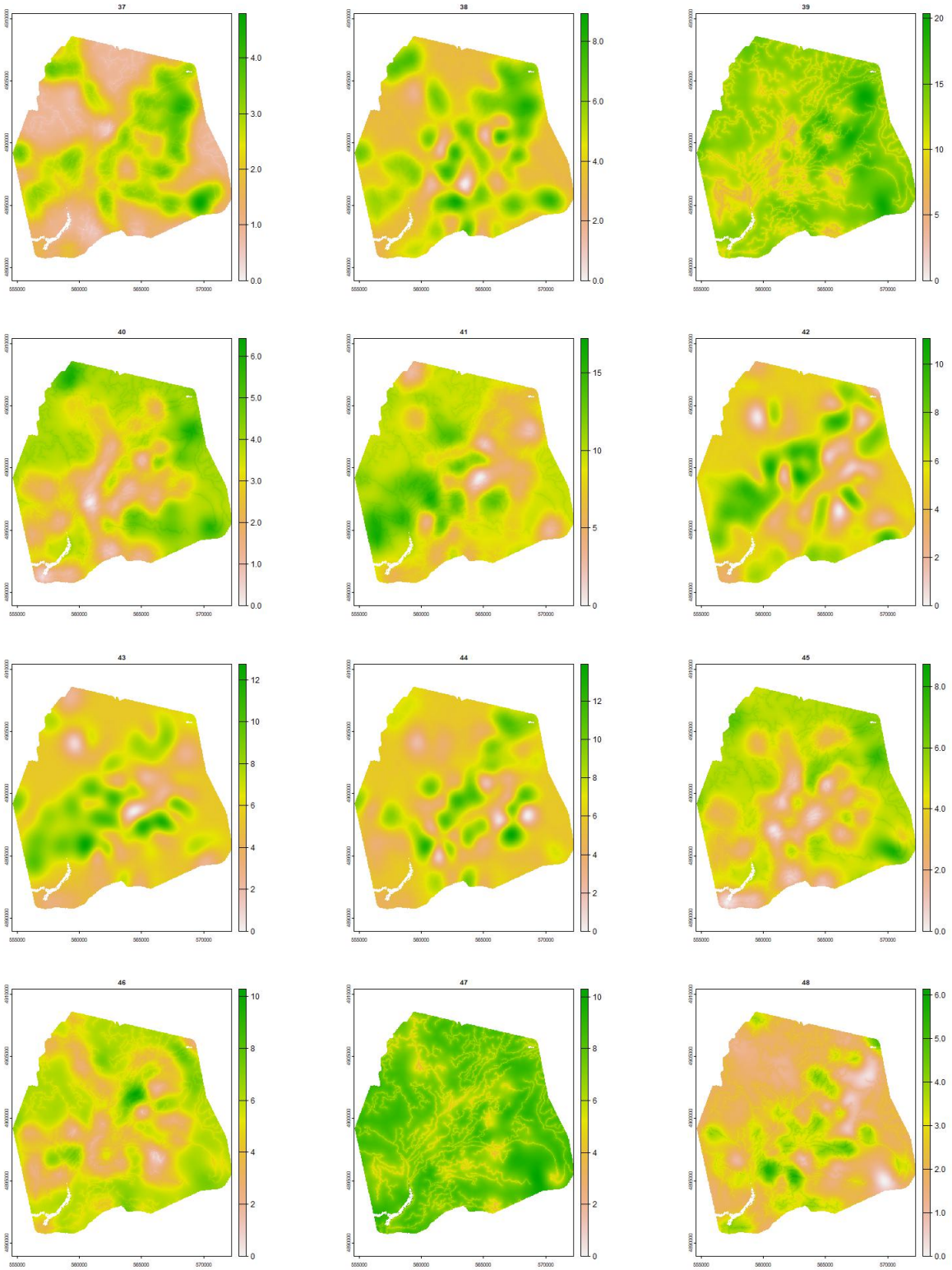

Figure 6: Maps of posterior mean log-biomass for species 37 to 48.

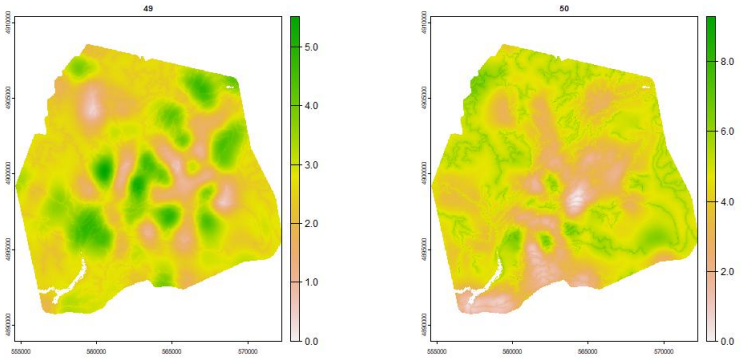

Figure 7: Maps of posterior mean log-biomass for species 49 to 50.

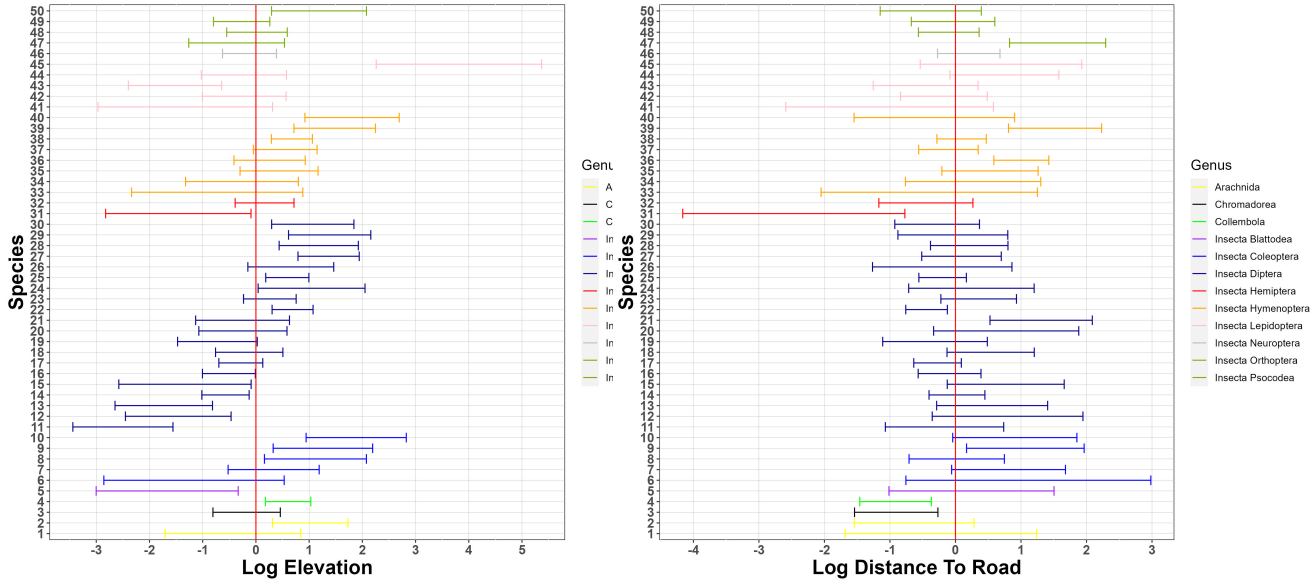

Figure 8: Results from gllvm: 95% PCI of the species-specific coefficients of log elevation (left) and distance to road (right) in the model for log-biomass. Species are grouped taxonomically.

6.2 Two stage occupancy model

We fit the two-stage occupancy model of Griffin et al. (2020):

$$\begin{cases} z_i^s \sim \text{Be}(\psi_i^s) \\ \text{logit}(\psi_i^s) = X_i \beta_s \\ \delta_{im}^s \sim \text{Be}(z_i^s \theta_{im}^s + (1 - z_i^s)\theta_0) \\ \text{logit}(\theta_i^s) = \beta_s^\theta \\ y_{imk}^s \sim \text{Be}(\delta_{im}^s p_s + (1 - \delta_{ijm}) q_s) \end{cases}$$

where:

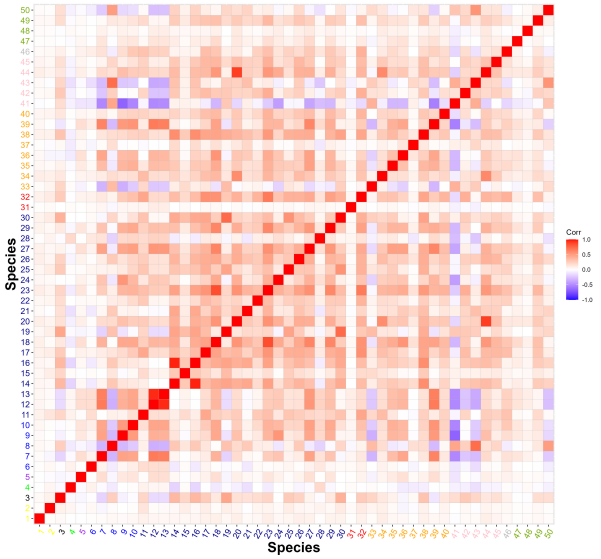

Figure 9: Results from gllvm: Correlation plot of all species. Red represents positive correlations while blue represents negative correlations. Species are grouped taxonomically.

- ψ is the occupancy probability;
- θ is the true positive probability at Stage 1;
- θ_0 is the false positive probability at Stage 1;
- p is the true positive probability at Stage 2;
- q is the false positive probability at Stage 2;

As before, we used as covariates the log-elevation and log-distance to road and summarise the estimated coeffiecients in Fig. 10.

7 Proof of study design results

7.1 Lemmas

We are going to denote by I_n the identity matrix of dimension n, the $n \times k$ matrix filled with 1's by $A_{n,k}$ and as $\mathbf{1}_{n,k}$ the $n \times nk$ matrix having 1's in the positions $(i, k(i-1)+1, \ldots, k(i-1)+k)$, $i = 1, \ldots, n$ and 0 everywhere else.

Lemma 7.1.

$$(a_1 I_n + a_2 A_{n,n})^{-1} = \frac{1}{a_1} I_n - \frac{a_2}{a_1(a_1 + n a_2)} A_{n,n}$$

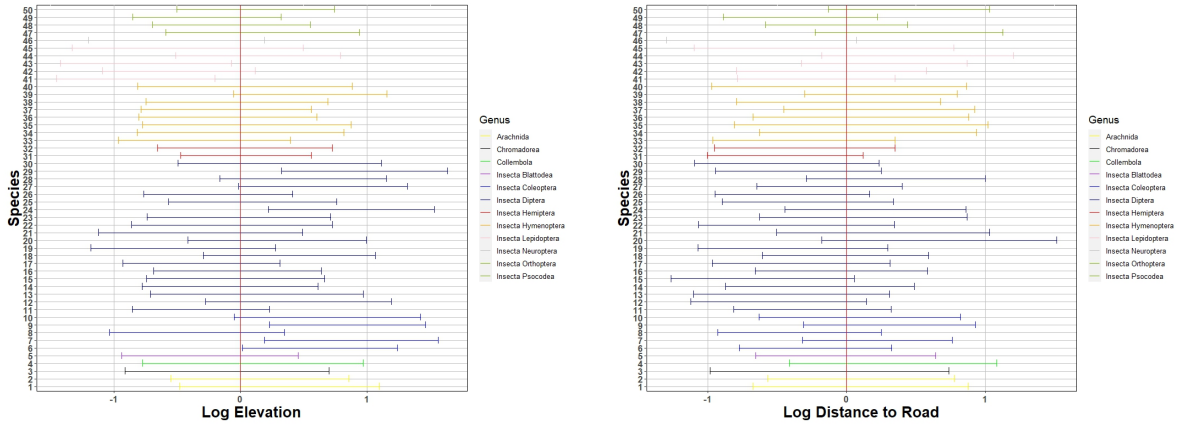

Figure 10: Results from the two-stage occupancy model: 95% PCI of the species-specific coefficients of log elevation (left) and distance to road (right) in the model for log-biomass. Species are grouped taxonomically.

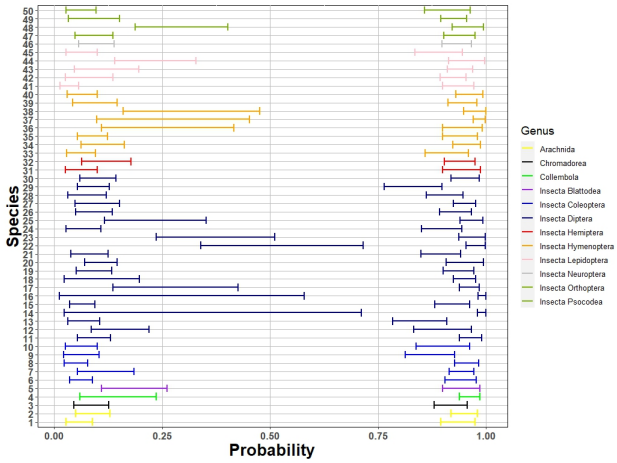

Figure 11: Results from the two-stage occupancy model: false positives and false negatives rate at the lab stage. Species are grouped taxonomically.

Lemma 7.2. *Let*

$$\begin{cases} y_i \sim N(x, \sigma^2) & i = 1, \dots, n \\ x \sim N(\mu, \tau^2) \end{cases}$$

Then $(y_1, \dots, y_n) \sim N(\mu, Q^{-1})$, *where* $Q = a_Q I + b_Q A_n$, *with* $a_Q = \frac{1}{\sigma^2}$, $b_Q = -\frac{\tau^2}{\sigma^2(\tau^2 n + \sigma^2)}$.

Lemma 7.3. *Let* y_i *be a* k *vector and* x *a scalar and*

$$\begin{cases} y_i \sim N(\mathbf{1}x, \Sigma) & i = 1, \dots, n \\ x \sim N(\mu, \tau^2) \end{cases}$$

Then $(y_1, \dots, y_n) \sim N(\mu, Q^{-1})$, *where* $Q = I_n \otimes \Sigma^{-1} - A_{n,n} \otimes \Sigma^{-1} a_\tau A_{k,k} \Sigma^{-1}$, *where* $a_\tau =$

$\frac{1}{n\sum_{l,k}\Sigma_{l,k}^{-1}+\frac{1}{\tau^2}}$.

Lemma 7.4. *Let Σ_i be a $k \times k$ matrix and x a k vector, if*

$$\begin{cases} y_i \sim N(x, \Sigma_i) \\ x \sim N(\mu, \tau^2 I) \end{cases}$$

then $(y_1, \ldots, y_n) \sim N(\mu, Q^{-1})$, *where* $Q = \begin{bmatrix} \Sigma_1^{-1} & \cdots & 0 \\ \vdots & \ddots & \vdots \\ 0 & \cdots & \Sigma_n^{-1} \end{bmatrix} - \begin{bmatrix} \Sigma_1^{-1}\Lambda_\tau\Sigma_1^{-1} & \cdots & \Sigma_n^{-1}\Lambda_\tau\Sigma_1^{-1} \\ \vdots & \ddots & \vdots \\ \Sigma_n^{-1}\Lambda_\tau\Sigma_n^{-1} & \cdots & \Sigma_n^{-1}\Lambda_\tau\Sigma_n^{-1} \end{bmatrix}$

and $\Lambda_\tau^{-1} = (\sum_i \Sigma_i^{-1} + \frac{1}{\tau^2} I_k)$

Lemma 7.5. *Let λ be a $1 \times n$ vector and Σ a $nk \times nk$ matrix. If*

$$\begin{cases} y \sim N(\lambda \mathbf{1}_{n,nk}, \Sigma) \\ \lambda \sim N(\mu, \tau^2 I) \end{cases}$$

then $y \sim N(0, Q^{-1})$, *where* $Q = \Sigma^{-1} - \Sigma^{-1}\mathbf{1}^T\Lambda_\tau^{-1}\mathbf{1}\Sigma^{-1}$, *with* $\Lambda_\tau = (\mathbf{1}\Sigma^{-1}\mathbf{1}^T + \frac{1}{\tau^2} I_n)$.

Lemma 7.6. *Let*

$$A = \begin{bmatrix} a_1 I_{n_1} & 0 & 0 \\ 0 & a_2 I_{n_2} & 0 \\ 0 & 0 & a_3 I_{n_3} \end{bmatrix} - \begin{bmatrix} b_{11} A_{n_1,n_1} & b_{12} A_{n_1,n_2} & b_{13} A_{n_1,n_3} \\ b_{21} A_{n_2,n_1} & b_{22} A_{n_2,n_2} & b_{23} A_{n_2,n_3} \\ b_{31} A_{n_3,n_1} & b_{32} A_{n_3,n_2} & b_{33} A_{n_3,n_3} \end{bmatrix},$$

Then,

$$A^{-1} = \begin{bmatrix} c_1 I_{n_1} & 0 & 0 \\ 0 & c_2 I_{n_2} & 0 \\ 0 & 0 & c_3 I_{n_3} \end{bmatrix} - \begin{bmatrix} d_{11} A_{n_1,n_1} & d_{12} A_{n_1,n_2} & d_{13} A_{n_1,n_3} \\ d_{21} A_{n_2,n_1} & d_{22} A_{n_2,n_2} & d_{23} A_{n_2,n_3} \\ d_{31} A_{n_3,n_1} & d_{32} A_{n_3,n_2} & d_{33} A_{n_3,n_3} \end{bmatrix},$$

7.2 Proof

In this subsection 6.1, we prove result (5) and (6) of the paper. First, we state the result.

Proposition. *Consider the model*

$$\begin{cases} v_{im}^s \sim N(l_i^s, \sigma^2) & i=1,\dots,n \quad m=1,\dots,M \quad s=1,\dots,S \\ v_{im}^s = 0 & i=1,\dots,n \quad m=1,\dots,M \quad s=S+1,\dots,S+S^\star \\ u_{imk} \sim N(0,\sigma_u^2) & i=1,\dots,n \quad m=1,\dots,M \quad k=1,\dots,K \\ \lambda_s \sim N(0,\sigma_\lambda^2) & s=1,\dots,S+S^\star \\ y_{imk}^s \sim N(u_{imk}+\lambda_s+v_{im}^s,\sigma_y^2) & i=1,\dots,n \quad k=1,\dots,K \quad s=1,\dots,S+S^\star \end{cases}$$

Then

$$\mathrm{Var}(l_1^s - l_2^s|y) = \frac{1}{M}\left(\sigma^2 + \frac{\sigma_y^2}{K}\left(1 + \frac{\frac{\sigma_u^2}{\sigma_y^2}}{\frac{\sigma_u^2}{\sigma_y^2}S^\star + 1}\right)\right). \tag{1}$$

If we assume that

$$l_i^s \sim N(X_i\beta, \tau^2) \qquad i=1,\dots,n \quad s=1,\dots,S$$

and $\sigma_\lambda^2 \gg \max\{\sigma_u^2, \sigma^2, \sigma_y^2\}$*, to obtain*

$$\mathrm{Var}(\beta|y) = \frac{1}{n-1}\left(\tau^2 + \frac{1}{M}\left(\sigma^2 + \frac{\sigma_y^2}{K}\right)\right)\left(1 + \frac{\sigma_u^2}{\sigma_y^2 + (M\tau^2+\sigma^2)K(1+S^\star\frac{\sigma_u^2}{\sigma_y^2}) + \sigma_u^2(S+S^\star-1)}\right). \tag{2}$$

7.3 Proof

First, we prove result (1). Given $\lambda = (\lambda_1,\dots,\lambda_S)$, $u = (u_{imk})$, $l_\cdot^S = (l_1^S,\dots,l_n^S)$, we have $p(y|l_\cdot^S) =$

$$\underbrace{\int p(\lambda)\int p(u)\underbrace{\left(\int \prod_{s=1}^{S-1} p(l_i^s)\int \prod_{s=1}^{S}\left[p(v_{im}^s|l_i^s)\prod_{i,m,k} p(y_{imk}^s|\lambda_s, v_{imk}^s, u_{imk})\right] dv dl^{-S}\right)}_{(a)}\underbrace{\left(\prod_{s=S+1}^{S+S^\star}\prod_{i,m,k} p(y_{imk}^s|\lambda_s,u_{imk})\right)}_{(b)} du\, d\lambda}_{(c)}$$

We first focus on (a). Using Lemma 7.2

$$\int p(v_{im}^s|l_i^s)\prod_k p(y_{imk}^s|u_{imk},\lambda_s,v_{im}^s)\,dv_{im}^s = N(y_{im\cdot}^s|l_i^s+u_{im\cdot}+\lambda_s,Q_1^{-1})$$

where $Q_1 = a_{Q_1}I_K + b_{Q_1}A_K$ with $a_{Q_1} = \frac{1}{\sigma_y^2}$ and $b_{Q_1} = -\frac{\sigma_v^2}{\sigma_y^2(\sigma_v^2K+\sigma_y^2)}$, so that

$$(a) = \left(\prod_{s=1}^{S-1}\prod_{i=1}^{n}\int p(l_i^s)\prod_{m=1}^{M}N(y_{im\cdot}^s|l_i^s+u_{im\cdot}+\lambda_s,Q_1^{-1})\,dl_i^s\right)\prod_{i=1}^{n}\prod_{m=1}^{M}N(y_{im\cdot}^S|l_i^S+u_{im\cdot}+\lambda_s,I_K)$$

Using Lemma 7.3, $\int p(l_i^s)\prod_{m=1}^{M}N(y_{im\cdot}^s|l_i^s+u_{im\cdot}+\lambda_s,Q_1^{-1})\,dl_i^s = \mathrm{N}(y_{i\cdot\cdot}^s|u_{i\cdot\cdot}+\lambda_s,Q_2^{-1})$, where $Q_2 = I_M\otimes Q_1 - A_{M,M}\otimes a_l(Q_1A_{K,K}Q_1)$, with a_l defined in the Lemma. Therefore,

$$\begin{aligned}(a) &= \left(\prod_{s=1}^{S-1}\prod_{i=1}^{n}\mathrm{N}(y_{i\cdot\cdot}^s|u_{i\cdot\cdot}+\lambda_s,Q_2^{-1})\right)\prod_{i=1}^{n}\mathrm{N}(y_{i\cdot\cdot}^S|l_i^Su_{i\cdot\cdot}+\lambda_s,\underbrace{I_M\otimes I_K}_{\hat{Q}_2^{-1}}))\\ &= \left(\prod_{s=1}^{S-1}\mathrm{N}(y_{\cdot\cdot\cdot}^s|u_{i\cdot\cdot}+\lambda_s,\underbrace{I_n\otimes Q_2^{-1}}_{Q_3^{-1}})\right)\mathrm{N}(y_{\cdot\cdot\cdot}^S|l_{\cdot}^S+u_{i\cdot\cdot}+\lambda_s,\underbrace{I_n\otimes\hat{Q}_2^{-1}}_{\hat{Q}_3^{-1}})\end{aligned}$$

while, (b) can be written as $\prod_{s=S+1}^{S+S^\star}\prod_{i,m,k}p(y_{\cdot\cdot}^s|\lambda_s+u_{imk}) = N(\lambda_s+u|\underbrace{I_n\underbrace{\otimes I_M\otimes(Q_1^\star)^{-1}}_{(Q_2^\star)^{-1}}}_{(Q_3^\star)^{-1}})$, with $Q_1^\star = \frac{1}{\sigma_y^2}I_K = a_{Q_1^\star}I_K$.

Therefore, $(c) =$

$$\int p(u)\left(\prod_{s=1}^{S-1}\mathrm{N}(y_{\cdot\cdot\cdot}^s|u_{i\cdot\cdot}+\lambda_s,Q_3^{-1})\right)\mathrm{N}(y_{\cdot\cdot\cdot}^S|l_{\cdot}^S+u_{i\cdot\cdot}+\lambda_s,\hat{Q}_3^{-1})\left(\prod_{s=S+1}^{S+S^\star}N(y_{\cdot\cdot\cdot}^s|u+\lambda_s,(Q_3^\star)^{-1})\right)du$$

Using Lemma 7.4, this is equal to $\mathrm{N}((0,l_{\cdot}^S,0)+\lambda,Q_4^{-1})$, where

$$Q_4 = \begin{bmatrix} I_{S-1}\otimes Q_3 & 0 & 0\\ 0 & \hat{Q}_3 & 0\\ 0 & 0 & I_{S^\star}\otimes Q_3^\star\end{bmatrix} -$$

$$\begin{bmatrix} A_{S-1,S-1}\otimes(Q_3\Lambda_u^{-1}Q_3) & A_{S-1,1}(Q_3\Lambda_u^{-1}\hat{Q}_3) & A_{S-1,S^\star}\otimes(Q_3\Lambda_u^{-1}Q_3^\star)\\ A_{1,S-1}\otimes(\hat{Q}_3\Lambda_u^{-1}Q_3) & (\hat{Q}_3\Lambda_u^{-1}\hat{Q}_3) & A_{1,S^\star}\otimes(\hat{Q}_3\Lambda_u^{-1}Q_3^\star)\\ A_{S^\star,S-1}\otimes(Q_3^\star\Lambda_u^{-1}Q_3) & A_{S^\star,1}(\hat{Q}_3\Lambda_u^{-1}Q_3) & A_{S^\star,S^\star}\otimes(Q_3^\star\Lambda_u^{-1}Q_3^\star)\end{bmatrix}$$

and $\Lambda_u = ((S-1)Q_3+\hat{Q}_3+S^\star Q_3^\star+\frac{1}{\sigma_u^2}I_{nMK})^{-1}$. Therefore, $p(y|l_{\cdot}^S)\propto$

$$\int p(\lambda)N(y_{1\cdot\cdot},\ldots,y_{S+S^\star\cdot\cdot}|(0,l_{\cdot}^S,0)+\lambda,Q_4^{-1})d\lambda$$

and finally, using Lemma 7.5, $p(y|l_{\cdot}^{S}) \sim \mathrm{N}((0, \mathbf{1}_{n,nMK}^{T} l_{\cdot}^{S}, 0), Q_5^{-1})$, where

$$Q_5 = Q_4 - Q_4 \mathbf{1}_{(S+S^\star),nMK(S+S^\star)}^{T} \Lambda_\lambda^{-1} \mathbf{1}_{(S+S^\star),nMK(S+S^\star)} Q_4,$$

and

$$\Lambda_\lambda = (\mathbf{1}_{(S+S^\star),nMK(S+S^\star)} Q_4 \mathbf{1}_{(S+S^\star),nMK(S+S^\star)}^{T} + \frac{1}{\sigma_\lambda^2} I_{(S+S^\star)})^{-1}.$$

Having derived an expression for $p(y|l_{\cdot}^{S})$, we can easily derive $Var(l_{\cdot}^{S}|y)$ but it's convenient to derive an expression for Q_5 in terms of M, K, n and $S^\star$.

We have $Q_2 = I_M \otimes Q_1 - A_{M,M} \otimes a_l(Q_1 A_{K,K} Q_1)$, which after expanding can be written as $a_{Q_2}(I_M \otimes I_K) + b_{Q_2}(I_M \otimes A_{K,K}) + c_{Q_2}(A_{M,M} \otimes A_{K,K})$ and similar relationship can be obtained for $\hat{Q}_2$ and $Q_2^\star$.

Next, since

$$\begin{aligned}
\Lambda_u =& I_n \otimes ((S-1)Q_2 + \hat{Q}_2 + S^\star Q_2^\star + \frac{1}{\sigma_u^2} I_{nMK})^{-1} \\
=& (S-1)\left(a_{Q_2}(I_M \otimes I_K) + b_{Q_2}(I_M \otimes A_{K,K}) + c_{Q_2}(A_{M,M} \otimes A_{K,K})\right) \\
&+ \left(a_{\hat{Q}_2}(I_M \otimes I_K) + b_{\hat{Q}_2}(I_M \otimes A_{K,K}) + c_{\hat{Q}_2}(A_{M,M} \otimes A_{K,K})\right) \\
&+ S^\star \left(a_{Q_2^\star}(I_M \otimes I_K) + b_{Q_2^\star}(I_M \otimes A_{K,K}) + c_{Q_2^\star}(A_{M,M} \otimes A_{K,K})\right) + \frac{1}{\sigma_u^2} I_{MK},
\end{aligned}$$

we can write Λ_u^{-1} as $I_n \otimes \underbrace{(a_u(I_M \otimes I_K) + b_u(I_M \otimes A_K) + c_u(A_M \otimes A_K))}_{(\Lambda_u^{-1})_0}$.

We can write Q_4 as $P - R$, where

$$P = \begin{bmatrix} I_{S-1} \otimes Q_3 & 0 & 0 \\ 0 & \hat{Q}_3 & 0 \\ 0 & 0 & I_{S^\star} \otimes Q_3^\star \end{bmatrix},$$

$$R = \begin{bmatrix} A_{S-1,S-1} \otimes I_n \otimes R_{11} & A_{S-1,1} \otimes I_n \otimes R_{12} & A_{S-1,S^\star} \otimes I_n \otimes R_{13} \\ A_{1,S-1} \otimes I_n \otimes R_{21} & I_n \otimes R_{22} & A_{1,S^\star} \otimes I_n \otimes R_{23} \\ A_{S^\star,S-1} \otimes I_n \otimes R_{13} & A_{S^\star,1} \otimes I_n \otimes R_{32} & A_{S^\star,S^\star} \otimes I_n \otimes R_{33} \end{bmatrix},$$

and $R_{ij} = G_i(\Lambda_u^{-1})_0 G_j$ (where $G_1 = Q_2$, $G_2 = \tilde{Q}_2$, $G_3 = Q_2^\star$), which can be written as $a_{r_{ij}} I_{MK} + b_{r_{ij}}(I_M \otimes A_{K,K}) + c_{r_{ij}} A_{MK,MK}$. Therefore,

$$\mathbf{1}_{(S+S^\star),nMK(S+S^\star)} P \mathbf{1}_{(S+S^\star),nMK(S+S^\star)}^{T} = \begin{bmatrix} (n\sum Q_2) I_S & 0 & 0 \\ 0 & (n\sum \hat{Q}_2) & 0 \\ 0 & 0 & (n\sum Q_2^\star) I_{S^\star} \end{bmatrix}$$

and

$$\mathbf{1}_{(S+S^\star),nMK(S+S^\star)}\, R\, \mathbf{1}^T_{(S+S^\star),nMK(S+S^\star)} = \begin{bmatrix} (n\sum R_{11})\, A_{S-1,S-1} & (n\sum R_{12})\, A_{S-1,1} & (n\sum R_{13}) A_{S-1,S^\star} \\ (n\sum R_{21})\, A_{1,S-1} & n\sum R_{22} & (n\sum R_{23})\, A_{1,S^\star} \\ (n\sum R_{13})\, A_{S^\star,S-1} & (n\sum R_{32})\, A_{S^\star,1} & (n\sum R_{33})\, A_{S^\star,S^\star} \end{bmatrix}$$

and hence Λ_λ can be written as

$$\begin{bmatrix} a_1^\lambda\, I_S & 0 & 0 \\ 0 & a_2^\lambda & 0 \\ 0 & 0 & a_3^\lambda\, I_{S^\star} \end{bmatrix} - \begin{bmatrix} b_{11}^\lambda\, A_{S-1,S-1} & b_{12}^\lambda\, A_{S-1,1} & b_{13}^\lambda\, A_{S-1,S^\star} \\ b_{21}^\lambda\, A_{1,S-1} & b_{22}^\lambda & b_{23}^\lambda\, A_{1,S^\star} \\ b_{31}^\lambda\, A_{S^\star,S-1} & b_{32}^\lambda\, A_{S^\star,1} & b_{33}^\lambda\, A_{S^\star,S^\star} \end{bmatrix}$$

with $a_1^\lambda = (n\sum Q_2 + \frac{1}{\sigma_\lambda^2})$, $a_2^\lambda = (n\sum \hat{Q}_2 + \frac{1}{\sigma_\lambda^2})$, $a_3^\lambda = (n\sum Q_3^\star + \frac{1}{\sigma_\lambda^2})$, and $b_{ij}^\lambda = n\sum R_{ij}$. Therefore,

$$\Lambda_\lambda^{-1} = \underbrace{\begin{bmatrix} c_1^\lambda\, I_S & 0 & 0 \\ 0 & c_2^\lambda & 0 \\ 0 & 0 & c_3^\lambda\, I_{S^\star} \end{bmatrix}}_{K_1} - \underbrace{\begin{bmatrix} d_{11}^\lambda\, A_{S-1,S-1} & d_{12}^\lambda\, A_{S-1,1} & d_{13}^\lambda\, A_{S-1,S^\star} \\ d_{12}^\lambda\, A_{1,S-1} & d_{22}^\lambda & d_{23}^\lambda\, A_{1,S^\star} \\ d_{13}^\lambda\, A_{S^\star,S-1} & d_{32}^\lambda\, A_{S^\star,1} & d_{33}^\lambda\, A_{S^\star,S^\star} \end{bmatrix}}_{K_2}$$

with coefficients defined as in Lemma 7.6.

Next, $Q_4\, \mathbf{1}^T_{(S+S^\star),nMK(S+S^\star)} = P\, \mathbf{1}^T_{(S+S^\star),nMK(S+S^\star)} - R\, \mathbf{1}^T_{(S+S^\star),nMK(S+S^\star)}$, where

$$H_1 := P\, \mathbf{1}^T_{(S+S^\star),nMK(S+S^\star)} = \begin{bmatrix} d_{Q_2}\, \mathbf{1}^T_{S-1,nMK(S-1)} & 0 & 0 \\ 0 & d_{\tilde{Q}_2}\, \mathbf{1}^T_{1,nMK} & 0 \\ 0 & 0 & d_{Q_2^\star}\, \mathbf{1}^T_{S^\star,nMKS^\star} \end{bmatrix}$$

where $d_{Q_2} = a_{Q_2} + Kb_{Q_2} + c_{Q_2}MK$ and similarly for $d_{Q_2^\star}$ and $d_{\tilde{Q}_2}$, and

$$H_2 := R\, \mathbf{1}^T_{(S+S^\star),nMK(S+S^\star)} = \begin{bmatrix} d_{R_{11}}\, A_{nMK(S-1),S-1} & d_{R_{12}}\, A_{nMKS,1} & d_{R_{13}}\, A_{nMKS,S^\star} \\ d_{R_{21}}\, A_{nMK,S} & d_{R_{22}}\, A_{nMK,1} & d_{R_{23}}\, A_{nMK,S^\star} \\ d_{R_{31}}\, A_{nMKS^\star,S} & d_{R_{32}}\, A_{nMKS^\star,1} & d_{R_{33}}\, A_{nMKS^\star,S^\star} \end{bmatrix}$$

where $d_{R_{ij}} = a_{R_{ij}} + Kb_{R_{ij}} + MKc_{R_{ij}}$ and similarly for the others. Therefore, $Q_4\, \mathbf{1}^T_{(S+S^\star),nMK(S+S^\star)}\, \Lambda_\lambda^{-1} = \left(P\, \mathbf{1}^T_{(S+S^\star),nMK(S+S^\star)} - R\, \mathbf{1}^T_{(S+S^\star),nMK(S+S^\star)}\right)(K_1 - K_2) = (H_1 - H_2)(K_1 - K_2)$. We have

$$H_1 K_1 = \begin{bmatrix} c_1^\lambda\, d_{Q_2}\, \mathbf{1}^T_{S-1,nMKS} & 0 & 0 \\ 0 & c_2^\lambda\, d_{\tilde{Q}_2}\, \mathbf{1}^T_{1,nMK} & 0 \\ 0 & 0 & c_3^\lambda\, d_{Q_2^\star}\, \mathbf{1}^T_{S^\star,nMKS^\star} \end{bmatrix},$$

$$H_1K_2 = \begin{bmatrix} c_1^\lambda\, d_{R_{11}}\, A_{nKS,S} & c_2^\lambda\, d_{R_{12}}\, A_{nKS,S^\star} & c_3^\lambda\, d_{R_{13}}\, A_{nKS,S^\star} \\ c_1^\lambda\, d_{R_{21}}\, A_{nKS^\star,S} & c_2^\lambda\, d_{R_{22}}\, A_{nKS^\star,S^\star} & c_3^\lambda\, d_{R_{23}}\, A_{nKS^\star,S^\star} \\ c_1^\lambda\, d_{R_{31}}\, A_{nKS^\star,S} & c_2^\lambda\, d_{R_{32}}\, A_{nKS^\star,S^\star} & c_3^\lambda\, d_{R_{33}}\, A_{nKS^\star,S^\star} \end{bmatrix},$$

$$H_2K_1 = \begin{bmatrix} d_{Q_2}\, d_{11}^\lambda\, A_{nK(S-1),S-1} & d_{Q_2}\, d_{12}^\lambda\, A_{nK,S^\star} & d_{Q_2}\, d_{13}^\lambda\, A_{nK(S-1),S^\star} \\ d_{\tilde{Q}_2}\, d_{11}^\lambda\, A_{nK(S-1),S^\star} & d_{\tilde{Q}_2}\, d_{12}^\lambda\, A_{nK,S^\star} & d_{\tilde{Q}_2}\, d_{13}^\lambda\, A_{nK(S-1),S^\star} \\ d_{Q_1^\star}\, d_{21}^\lambda\, A_{nKS^\star,S} & d_{Q_1^\star}\, d_{22}^\lambda\, A_{nKS^\star,S^\star} & d_{Q_1^\star}\, d_{22}^\lambda\, A_{nKS^\star,S^\star} \end{bmatrix},$$

and

$$H_2K_2 = \begin{bmatrix} M^\star_{S,1,1} & M^\star_{S^\star,1,2} & M^\star_{S^\star,1,3} \\ M^\star_{S,2,1} & M^\star_{S^\star,2,2} & M^\star_{S^\star,2,3} \\ M^\star_{S,3,1} & M^\star_{S^\star,3,3} & M^\star_{S^\star,3,3} \end{bmatrix} \text{ where } M^\star_{T,i,j} = A_{nKS,T}(d_{R_{i1}}\, d_{1j}^\lambda\, S + d_{R_{i2}}\, d_{2j}^\lambda + d_{R_{i3}}\, d^{\lambda_{3j}})\, S^\star.$$

Implying that

$$Q_4\, \mathbf{1}^T_{S,nKS}\, \Lambda_\lambda^{-1} = \underbrace{\begin{bmatrix} \mathbf{1}^T_{S,nKS} c_{\eta_1} & 0 & 0 \\ 0 & \mathbf{1}^T_{S^\star,nKS^\star} c_{\eta_2} & 0 \\ 0 & 0 & \mathbf{1}^T_{S^\star,nKS^\star} c_{\eta_3} \end{bmatrix}}_{J_1} - \underbrace{\begin{bmatrix} d_{\eta_{11}}\, A_{nKS,S} & d_{\eta_{12}}\, A_{nkS,S^\star} & d_{\eta_{13}}\, A_{nkS,S^\star} \\ d_{\eta_{21}}\, A_{nKS,S} & d_{\eta_{22}}\, A_{nkS,S^\star} & d_{\eta_{23}}\, A_{nkS,S^\star} \\ d_{\eta_{31}}\, A_{nKS,S} & d_{\eta_{32}}\, A_{nkS,S^\star} & d_{\eta_{33}}\, A_{nkS,S^\star} \end{bmatrix}}_{J_2}.$$

And finally,

$$J_1H_1^T = \begin{bmatrix} (c_{\eta_1} d_{Q_2})\; I_{S-1} \otimes A_{nMK,nMK} & 0 & 0 \\ 0 & \left(c_{\eta_2} d_{\hat{Q}_2}\right) A_{nMK,nMK} & 0 \\ 0 & 0 & \left(c_{\eta_3} d_{Q_2^\star}\right) I_{S^\star} \otimes A_{nMK,nMK} \end{bmatrix},$$

$$J_1H_2^T + J_2H_1^T = \begin{bmatrix} N^\star_{S-1,S-1,c_{\eta_1},R_{11},d_{\eta_{11}},Q_2} & N^\star_{S-1,1,c_{\eta_1},R_{12},d_{\eta_{12}},\tilde{Q}_2} & N^\star_{S-1,S^\star,c_{\eta_1},R_{13},d_{\eta_{13}},Q_2^\star} \\ N^\star_{1,S-1,c_{\eta_2},R_{21},d_{\eta_{21}},Q_2} & N^\star_{1,1,c_{\eta_2},R_{22},d_{\eta_{22}},\tilde{Q}_2} & N^\star_{1,S^\star,c_{\eta_2},R_{23},d_{\eta_{23}},\tilde{Q}_2} \\ N^\star_{S^\star,S-1,c_{\eta_3},R_{31},d_{\eta_{31}},Q_2} & N^\star_{S^\star,1,c_{\eta_3},R_{32},d_{\eta_{22}},\tilde{Q}_2} & N^\star_{S^\star,S^\star,c_{\eta_3},R_{33},d_{\eta_{33}},Q_2^\star} \end{bmatrix}$$

where $N^\star_{S_1,S_2,c_\eta,R,d_\eta,Q} = (c_\eta d_R + d_\eta d_Q)\; A_{nMKS_1,nMKS_2}$,

$$J_2^TH_2^T = \begin{bmatrix} A_{nMK(S-1,nMK(S-1)} t_{11} & A_{nMK(S-1),nMK} t_{12} & A_{nMK(S-1),nMKS^\star} t_{13} \\ A_{nMKS^\star,nMKS} t_{21} & A_{nMK^\star,nMK^\star} t_{22} & A_{nMK^\star,nMK^\star} t_{23} \\ A_{nMKS^\star,nMKS^\star} t_{31} & A_{nMKS^\star,nMK} t_{32} & A_{nMKS^\star,nMKS^\star} t_{33} \end{bmatrix}$$

where $t_{ij} = (S-1)d_{\eta_{i1}}d_{R_{1j}} + d_{\eta_{i2}}d_{R_{2j}} + S^\star d_{\eta_{i3}}d_{R_{3j}}$. This implies that

$$
\begin{aligned}
&Q_4\,\mathbf{1}_{S,nMKS}^T\,\Lambda_\lambda^{-1}\,\mathbf{1}_{S,nMKS}Q_4 \\
&= \begin{bmatrix} (c_{\eta_1}d_{Q_2})\; I_S \otimes A_{nMK,nMK} & 0 & 0 \\ 0 & \left(c_{\eta_2}d_{\tilde{Q}_2}\right)\; I_{S^\star} \otimes A_{nMK,nMK} & 0 \\ 0 & 0 & \left(c_{\eta_3}d_{Q_2^\star}\right)\; I_{S^\star} \otimes A_{nMK,nMK} \end{bmatrix} \\
&\quad - \begin{bmatrix} f_{11}\,A_{nMK(S-1),nMK(S-1)} & f_{12}\,A_{nMK(S-1),nMK} & f_{13}\,A_{nMK(S-1),nMKS^\star} \\ f_{21}\,A_{nMK,nMK(S-1)} & f_{22}\,A_{nMK,nMK} & f_{23}\,A_{nMK,nMKS^\star} \\ f_{31}\,A_{nMKS^\star,nMK(S-1)} & f_{32}\,A_{nMKS^\star,nMK} & f_{33}\,A_{nMKS^\star,nMKS^\star} \end{bmatrix}.
\end{aligned}
$$

From the expression for $p(y|l_\cdot^S)$, we obtain

$$Var(l_\cdot^S|y) = (\mathbf{1}_{n,nMK}\,(Q_5)_{nMK(S-1)+1,\ldots,nMK;nMK(S-1)+1,\ldots,nMK}\,\mathbf{1}_{n,nMK}^T)^{-1}$$

and, since

$$
\begin{aligned}
&\mathbf{1}_{n,nMK}\,(Q_5)_{nMK(S-1)+1,\ldots,nMK;nMK(S-1)+1,\ldots,nMK}\,\mathbf{1}_{n,nMK}^T \\
&= I_n\,\underbrace{(MK(a_{\tilde{Q}_2} - a_{R_{22}} + MK^2(b_{\tilde{Q}_2} - b_{R_{22}}) + M^2K^2(c_{\tilde{Q}_2} - c_{R_{22}}))}_{a_{Q_3}} + A_{n,n}\,\underbrace{(-M^2K^2(c_{\eta_2}d_{\tilde{Q}_2} - f_{22}))}_{b_{Q_3}},
\end{aligned}
$$

we obtain $Var(l_\cdot^S|y) = c_{Q_3}I_n + d_{Q_3}A_{n,n}$, where $c_{Q_3} = \frac{1}{a_{Q_3}}$ and so

$$Var(l_{1S} - l_{2S}) = 2(Var(l_{1S}) - \mathrm{Cov}(l_{1S}, l_{2S})) = 2c_{Q_3}.$$

To prove result (2), we need to compute $p(y|X\beta^S)$. We have that

$$\int p(\lambda) \int p(u) \underbrace{\left(\int \prod_{s=1}^{S-1} p(l_i^s) \int \prod_{s=1}^{S} \left[p(v_{im}^s) \prod_{i,m,k} p(y_{imk}^s|\lambda_s, v_{imk}^s, u_{imk}) \right] dv dl^{-S} \right)}_{(a)} \left(\prod_{s=S+1}^{S+S^\star} \int\int \prod_{i,m,k} p(y_{imk}^s|\lambda_s, u_{imk}) \right) d\lambda du}_{(b)}$$

With similar calculations to before, we obtain $y|X\beta^S \sim \mathrm{N}((0, (\mathbf{1}_{n,nMK}^T X\beta_s)^T, 0)^T, Q_5^{-1})$, where $Q_5 = Q_4 - Q_4\,\mathbf{1}_{S,nMKS}^T\,\Lambda_\lambda^{-1}\,\mathbf{1}_{S,nMKS}\,Q_4$.

Now, $\Lambda_u^{-1} = I_n \otimes (SQ_2 + S^\star Q_2^\star + \frac{1}{\sigma_u^2}I_{MK})^{-1}$. We have

$$
\begin{aligned}
SQ_2 + S^\star Q_2^\star + \frac{1}{\sigma_u^2}I_{nMK} = &S\,(a_{Q_2}(I_M \otimes I_K) + b_{Q_2}(I_M \otimes A_{K,K}) + c_{Q_2}(A_{M,M} \otimes A_{K,K})) \\
&+ S^\star\left(a_{Q_2^\star}(I_M \otimes I_K) + b_{Q_2^\star}(I_M \otimes A_{K,K}) + c_{Q_2^\star}(A_{M,M} \otimes A_{K,K})\right) + \frac{1}{\sigma_u^2}I_{MK}
\end{aligned}
$$

and therefore $\Lambda_u^{-1} = I_n \otimes \underbrace{(a_u(I_M \otimes I_K) + b_u(I_M \otimes A_K) + c_u(A_M \otimes A_K))}_{(\Lambda_u^{-1})_0}$.

From the expression for $p(y|\beta)$, we obtain

$$Var(\beta|y) = (X^T \mathbf{1}_{n,nMK}(Q_5)_{nMK(S-1)+1,\ldots,nMK;nMK(S-1)+1,\ldots,nMK} \mathbf{1}_{n,nMK}^T X)^{-1}$$

and since, with similar derivations as before, we can write $\mathbf{1}_{n,nMK}(Q_5)_{nMK(S-1)+1,\ldots,nMK;nMK(S-1)+1,\ldots,nMK}\mathbf{1}_{n,nMK}^T$ as $a_{Q_3} I_{n,n} + b_{Q_3} A_{n,n}$, we have $Var(\beta|y) = \frac{1}{(X^T X) a_{Q_3} + (\sum X)^2 b_{Q_3}}$. The final result can be obtained by noting that if $X_1, \ldots, X_n \overset{i.i.d.}{\sim} \mathrm{N}(0,1)$, then $\mathbf{E}[X^T X] = \mathbf{E}[(\sum X_i)^2] = n$.

References

J. E. Griffin, E. Matechou, A. S. Buxton, D. Bormpoudakis, and R. A. Griffiths. Modelling environmental DNA data; Bayesian variable selection accounting for false positive and false negative errors. *Journal of the Royal Statistical Society: Series C (Applied Statistics)*, 69(2):377–392, 2020.

Y. Li, B. A. Craig, and A. Bhadra. The graphical horseshoe estimator for inverse covariance matrices. *Journal of Computational and Graphical Statistics*, 28(3):747–757, 2019.

E. Makalic and D. F. Schmidt. A simple sampler for the horseshoe estimator. *IEEE Signal Processing Letters*, 23(1):179–182, 2015.

N. G. Polson, J. G. Scott, and J. Windle. Bayesian inference for logistic models using Pólya–Gamma latent variables. *Journal of the American Statistical Association*, 108(504):1339–1349, 2013.

H. Wang. Bayesian graphical lasso models and efficient posterior computation. *Bayesian Analysis*, 7(4): 867–886, 2012.